Cite this document as: *Soft Matter* 15 (2019) 1730-1746

Barrier kinetics of adsorption-desorption of alcohol monolayers on water under constant surface tension

Ivan L. Minkov,[a,b] Dimitrinka Arabadzhieva,[c] Ibrahim E. Salama,[d,e]
Elena Mileva,[c] Radomir I. Slavchov*[,f,g]

[a] *Department of Physical Chemistry, Faculty of Chemistry and Pharmacy, Sofia University, 1 J. Bourchier Blvd., 1164 Sofia, Bulgaria*
[b] *Department of Chemistry, Biochemistry, Physiology, and Pathophysiology, Faculty of Medicine, Sofia University, 1 Koziak Str., 1407 Sofia, Bulgaria*
[c] *Bulgarian Academy of Science, Akad. G. Bonchev Str., bl.11, 1113 Sofia, Bulgaria, Sofia, Bulgaria*
[d] *Department of Chemisty, Cambridge University, CB2 1EW Cambridge, United Kingdom*
[e] *BP Institute, Cambridge University, Bullard Laboratories, Madingley Road, CB3 0EZ Cambridge, United Kingdom*
[f] *Department of Chemical Engineering and Biotechnology, Cambridge University, Philippa Fawcett Drive, West Site, CB3 0AS Cambridge, United Kingdom*
[g] *School of Engineering and Materials Science, Queen Mary University of London, Mile End Road, London E1 4NS, United Kingdom*
**E-mail: ris26@cam.ac.uk*

Abstract: The desorption of spread decanol and dodecanol monolayers at controlled constant surface tension is shown to proceed under mixed barrier-diffusion control; the role of the convective diffusion is also discussed. The desorption rate is measured as a function of the density of the monolayer and the temperature. The rate of barrier desorption increases as the monolayer approaches the collapse point, reaching an infinite value. The average desorption time of an adsorbed dodecanol molecule increases linearly with the area per molecule, and is phase-specific – it is higher for the liquid condensed state of the monolayer than for the liquid expanded. The desorption rate increases with temperature; the activation energy for desorption is independent of the compression and the surface phase. The increase of the intensity of convection is shown to produce a vanishingly thin diffusion layer and causes the desorption to proceed under pure barrier control. A schematic map of the adsorption-desorption regimes acting as function of time and intensity of the convection is constructed. General expressions for the rate of adsorption and desorption of alcohols are formulated.

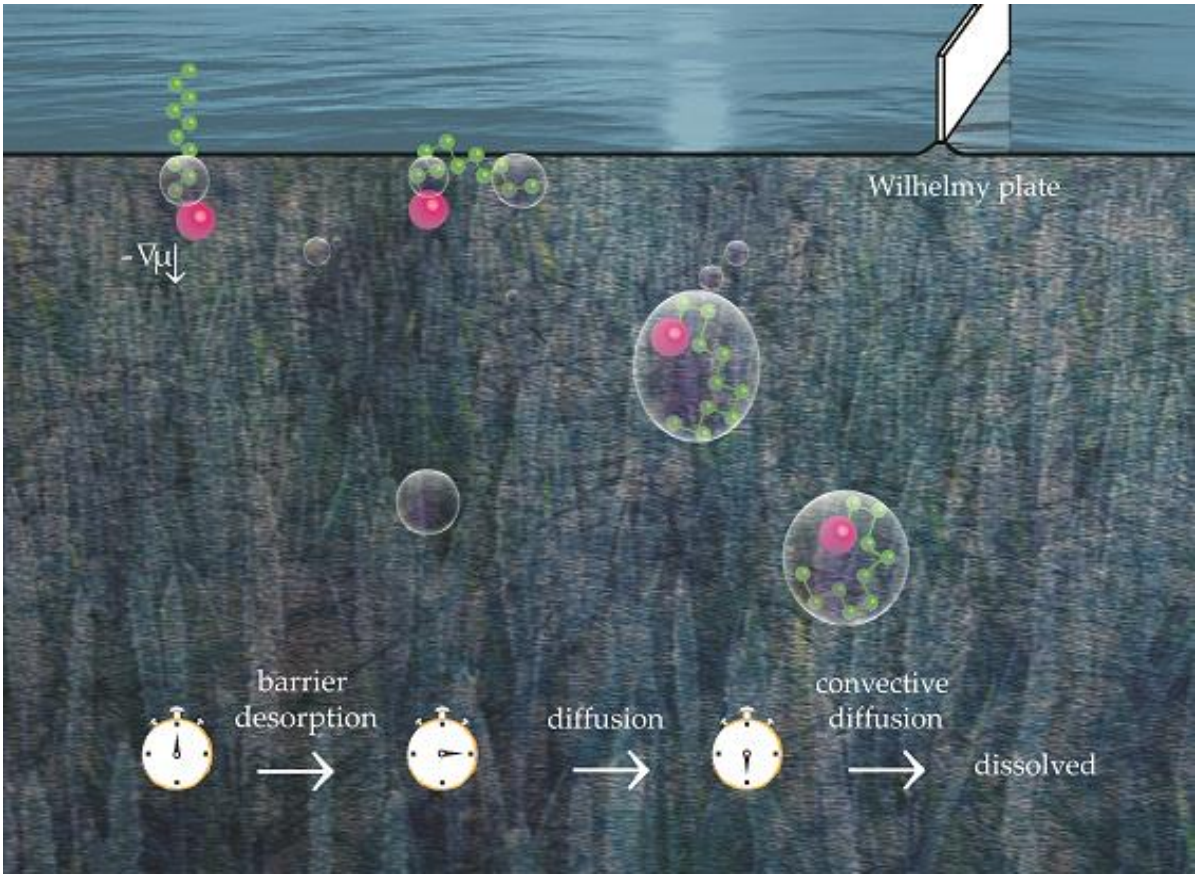

Decanol and dodecanol desorb from the surface of water following mixed barrier–diffusion kinetics. Convection accelerates the diffusion process to the point where desorption proceeds under pure barrier control, allowing accurate measurement of the rate parameters. Minkov et al. mapped the adsorption regimes as a function of convection intensity and time.

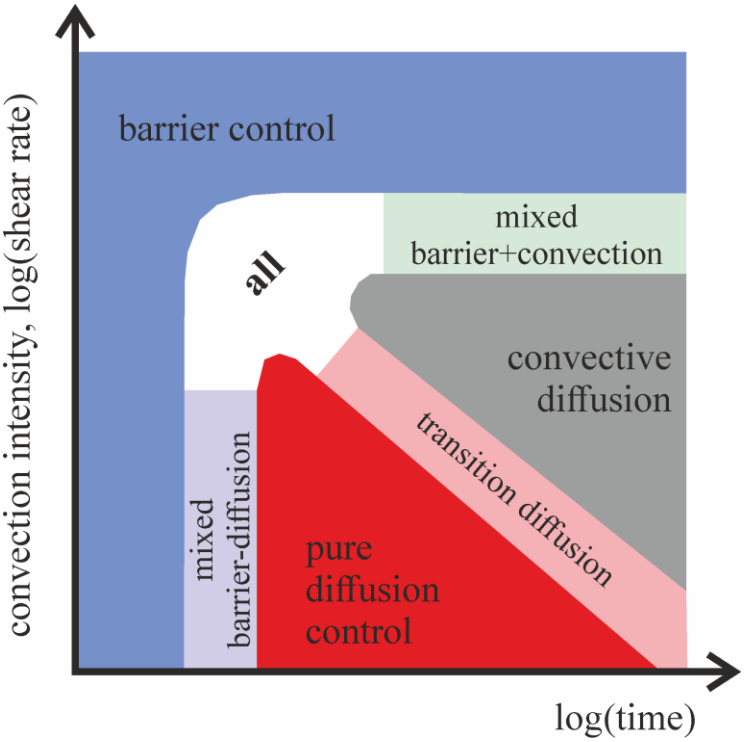

Keywords: Langmuir trough, spread monolayer, isobaric desorption, adsorption kinetics, adsorption barrier, non-ionic surfactants

1. Introduction

A common application [1-16] of the Langmuir trough is to follow the process of desorption of a spread monolayer of slightly soluble amphiphile under isobaric conditions, where the decrease of the area A of the film with time t is monitored at constant surface pressure π^S ($\pi^S = \sigma_0 - \sigma$, where σ_0 and σ are the surface tensions of the pure solvent and of the monolayer). The isobaric regime has been used for determination of the diffusion coefficient D of the surfactant [5] and for evaluation of its solubility [11]; to study the dissociation and the Hofmeister effect on the properties of monolayers of adsorbed acids [7]; to study the processes involved in the collapse of the monolayer [8,12]; phase transitions [14] in monolayers; interaction between adsorbed lipids and proteins [10]; and generally – the mechanism of desorption [4,6,9]. Recently, we used the isobaric regime as an auxiliary experiment to correct the π^S vs. A isotherms for the material loss due to dissolution of the monolayer [17] (similarly to Motomura et al. [18]). Incidentally, we found that these auxiliary data suggested characteristics of the desorption process in apparent disagreement with certain literature results; in particular, a surprisingly slow rate of barrier desorption of dodecanol off the surface was evident. These findings were the motivation to investigate the kinetics of the desorption process in more detail.

Most isobaric studies in the field report a **mechanism of the desorption** process proceeding in two stages. During the first minutes after the formation of the monolayer, the

desorption rate is controlled by a diffusion process, following approximately parabolic dependence of the area on time, $\ln(A_0/A) \propto t^{1/2}$, where A_0 is the initial area covered by the monolayer. We shall refer to this as *D-regime, pure diffusion control*, or $t^{1/2}$*-regime*. The rate-determining process of this stage is the diffusion of surfactant through a diffusion layer of a thickness increasing with time as $(Dt)^{1/2}$. After several minutes, another regime starts operating, where convection accelerates the diffusion and the desorption rate [3]. The approximate physical picture behind it was set by Ter Minassian-Saraga [3,4] (by analogy with the classical works on dissolution of solids [19] and diffusion-limited electrolysis [20]), and involves two layers: in the subphase next to the monolayer, a *stagnated layer* of liquid of thickness L_{st} exists, where the effect of the convection is negligible (Péclet number $Pe << 1$) and a stationary diffusion profile is established. Deeper in the bulk below the stagnated layer, another *convection layer* stands, where convection is assumed very efficient ($Pe >> 1$), causing concentration to be equilibrated to its bulk value. We refer to this picture as *C-regime*, *convective diffusion*. It leads to an approximately linear dependence $\ln(A_0/A) \propto t$. The transition from *D*- to C- regime occurs when $L_{st} \approx (Dt)^{1/2}$. De Keyser and Joos gave a theoretical expression for the stagnated layer thickness L_{st} for the case where the convection is caused by the trough's barrier movement [9]:

$$L_{st} = \left(\frac{\pi D}{2}\right)^{1/2} \left(\frac{\mathrm{d}\ln A}{\mathrm{d}t}\right)^{-1/2} \qquad \left(\sim \frac{D^{1/2}}{\mathrm{d}v_x/\mathrm{d}z}\right). \tag{1}$$

Another common source of stirring is the natural convection, where the shear $\mathrm{d}v_x/\mathrm{d}z$ in eqn (1) is caused by temperature gradients. The intensity of the convection can be regulated via the thickness of the substrate [8], and by tight control of the temperature in the system. More vigorous stirring causes thinning of the stagnated layer and faster dissolution (larger $|\mathrm{d}\ln A/\mathrm{d}t|$). Most studies in the literature [3-5,9-16] report data that transits from *D*- to C-regime.

A third regime has been reported to operate at short times [6]: while the diffusion layer is still thin, the rate determining process is the flip-flop-like desorption of surfactant from the monolayer to the solvent (τ_d*-regime*, *barrier control*). This regime leads again to a linear dependence $\ln(A_0/A) \propto t$, but the coefficient in it is related to the energy barrier for the transfer from the monolayer to the subsurface. This behaviour is typical for very large adsorbates (proteins, nanoparticles); however, Baret et al. found a significant effect from the barrier process already for decanol [6]. De Keyser and Joos [9] plainly repudiated the work of Baret et al. as erroneous and leading to "*the false conclusion that desorption is not controlled by diffusion*". This was a bold statement on their side, especially in view that the first few points (first 1-2 minutes) of their own experimental $A(t)$ curves often deviate from the $\ln(A_0/A) \propto t^{1/2}$ law, approaching $\ln(A_0/A) \propto t$ instead, which is an indication of a barrier rate process (cf. their *Fig. 1*). Miller and Lunkenheimer [21] also found no need of a barrier in their interpretation of desorption data for long-chained fatty alcohols and acids, and used dynamic surface tension data to determine the diffusion coefficients for these amphiphiles, but Motomura et al. determined a barrier rate constant for myristic acid [18] at pH 2. In our study [17] of dodecanol

monolayers spread on pure water or concentrated aqueous electrolytes, we found that the desorption is proceeding under barrier control for the initial 1-2 minutes. The apparent disagreements in the literature regarding the mechanism of adsorption and desorption is further discussed in the review by He et al. [22].

The three regimes (τ_d-, *D*- and C-) do not exhaust the possibilities. Mixed barrier-diffusion (τ_d & *D*-) and barrier-convective diffusion (τ_d & C-) control are common [6]. Other regimes have been reported, related to collapse and phase transition kinetics [8,12,23] instead of solubility. The desorption rate is affected strongly by the presence of micelles [24-26]. Evaporation is an important factor [27-30] that further complicates the desorption process. Hommelen [29] found that the surface tension of alcohol monolayers is a few mN/m lower when the surrounding air is saturated with the vapours of the alcohol solution, compared to the case where evaporation is taking place – *i.e.* evaporation leads to the establishment of a quasi-stationary alcohol adsorption lower than the equilibrium one. This effect is reversible within the first minutes of the experiment (if evaporation stops, the surface tension relaxes back to its equilibrium value), but becomes irreversible after several hours of evaporation due to decanol depletion [29]. Brooks and Alexander [27,28] reported that the increase of the salinity of the substrate does not change significantly the rate of desorption of fatty alcohols of chain length 14-18, which suggests that the loss of adsorbed material they observed is due to evaporation instead. On the other hand, the rate of desorption of $C_{12}H_{25}OH$ decreases with the increase of the electrolyte concentration, and a significant accumulation of dissolved surfactant in the aqueous phase is observed [17,31], which proves that most of this alcohol desorbs in the liquid phase (which does not exclude evaporation).

To summarize, the barrier process of desorption is a phenomenon that is far from being well understood. Its rate has a strong dependence on Γ that has not been studied in enough detail, and the data for it are discordant [32]. The studies of the effect of the temperature on the desorption rate are very limited (cf. ref. [24] for a brief review), and the activation energy of this process is known only to an order of magnitude. The problem is controversial – respected authors even denied the existence of a barrier process [9]. Combined with the high practical importance of the question, this makes the desorption under barrier control one of the most appealing fundamental problems in colloid science currently.

The main objectives of our study are to define the time limit between the τ_d- and *D*-regime; to evaluate the role of the convection; to re-analyse the results of Baret at al. [6] and de Keyser and Joos [9] and to compare them with ours, hopefully reconciling them; to measure the rate of barrier desorption as a function of the monolayer compression and the temperature, and to determine the desorption energetic barrier. Another important goal is to revive the desorption isobar method – most modern adsorption-desorption kinetic studies use other techniques to follow the process (mostly methods where the dynamic surface tension is recorded as a function of time at fixed area [21,24,33-36]), and the reviews in the field from the last 20 years [24,34,37]

hardly ever discuss this classical technique. The desorption isobars have an important advantage over the competing methods for monitoring desorption kinetics: the technique allows the process to be followed at constant π^S and density Γ of the monolayer, which simplifies significantly the interpretation of the data. In contrast, a model multiparametric dependence for the desorption rate as a function of Γ (*e.g.*, Frumkin's, Langmuir-Hinshelwood or their derivatives [34-41]) has to be postulated in advance with most dynamic surface tension studies. We also show how the accuracy of the barrier desorption rate measurement via the isobar technique can be improved by independent measurement of the other parameters involved in the desorption process (diffusion coefficient D and adsorption length Γ/C_{eq}).

The theory of the isobaric desorption under mixed barrier-diffusion regime is summarized in sec. 2. In sec. 3.1 & 3.2, we determine experimentally the solubility C_{eq} of the dodecanol monolayer as a function of Γ, and in sec. 3.3, the diffusion coefficient D is determined. The rate of desorption obtained from the desorption isobars is discussed in sec. 3.4; its dependence on Γ and T is experimentally investigated, and the activation energy for the flip-flop event is determined. We show that intensive convection can shrink the diffusion layer to negligible thickness, causing desorption under pure barrier regime. In sec. 4, our measurements are compared to literature data, and our results are summarized and presented in a schematic map of the regimes of adsorption-desorption as function of the intensity of convection and time.

2. Desorption in the isobaric regime under barrier-diffusion control: theory

In an isobaric desorption experiment, a surfactant monolayer is spread on the surface and then compressed quickly to a predefined value of the surface pressure π^S in a Langmuir trough. The monolayer is then left to dissolve; the material lost due to dissolution is precisely compensated for by compression of the monolayer – at each time step, the electronic control system adjusts the barrier position until the predefined π^S is restored. Under isobaric conditions, the desorption of a single-component homogeneous adsorption layer proceeds also under constant adsorption Γ and chemical potential of the monolayer μ, as the fixed value of the π^S defines Γ and μ through the equation of state of the monolayer. This assumption holds if (i) the characteristic time of the experiment is longer than the relaxation time of a monolayer of given density to its equilibrium state (fulfilled for small molecules such as dodecanol), and (ii) the bulk solution of surfactant is not concentrated (again fulfilled for dodecanol). A general discussion of the limitations of this assumption is available in ref. [42].

The driving force of the dissolution process is the difference in the chemical potential of the surfactant at the surface and in the bulk, or equivalently, between the *solubility of the*

monolayer C_{eq} and the *actual* surfactant bulk concentration of the substrate (which is 0). The chemical potential in the monolayer is related to Γ as

$$\mu = \mu_0^S + k_B T \ln \gamma^S \Gamma , \tag{2}$$

where γ^S is surface activity coefficient, μ_0^S is standard chemical potential of a surfactant molecule at the surface (a list of symbols is provided in the electronic supplement). The chemical potential μ can be calculated from the experimental surface pressure isotherm, $\pi^S(\Gamma)$, through the integral form of the Gibbs adsorption equation:

$$\Delta_s \mu \equiv \mu - \mu_s = \int_{\pi_s^S}^{\pi^S} \Gamma^{-1} \mathrm{d}\pi^S , \quad \text{where} \quad \mu_s = \mu_0^S + k_B T \ln \gamma_s^S \Gamma_s . \tag{3}$$

A graphical representation of this relation is given in Figure S17 in S4. Here, μ_s, π_s^S, Γ_s and γ_s^S refer to a suitably chosen standard state. A particularly convenient standard state is that of the monolayer in equilibrium with crystals of the surfactant [17,43]; in this case, π_s^S and μ_s are the spreading pressure and the chemical potential of surfactant crystals, Γ_s is the surface density of the monolayer spread around the crystals, and γ_s^S is its surface activity coefficient. The solubility C_{eq} of the monolayer is related to its density through the condition for equilibrium between the solution (of chemical potential $\mu_0^B + k_B T \ln C_{eq}$) and the monolayer [44,45], *i.e.* the adsorption isotherm

$$\gamma^S \Gamma = K_a C_{eq} \qquad (\gamma_s^S \Gamma_s = K_a C_s \text{ for the standard state}). \tag{4}$$

Here, $K_a = \exp[(\mu_0^B - \mu_0^S)/k_B T]$ is the *adsorption constant* of the surfactant; for our choice of standard state, C_s is the solubility of the surfactant crystals. From eqn (2)-(4) it follows that the solubility of the monolayer C_{eq} is related to the measurable quantity $\Delta_s \mu$ as:

$$C_{eq} = C_s \exp(\Delta_s \mu / k_B T) . \tag{5}$$

Thus, the knowledge of C_s, π_s^S, and the surface pressure vs. area isotherm allows the solubility of the monolayer at any compression to be calculated through eqn (3)&(5) (Figure S17 in S4).

Let us now consider the change of the area of the monolayer with time. We assume that the surfactant desorbs under mixed barrier-diffusion control [6] (τ_d & *D-regime*); convection is neglected, which makes the model applicable only to the initial period of the process when $t < L_{st}^2/D$. The evolution of the concentration profile in the bulk follows Fick's law,

$$\frac{\partial C}{\partial t} = D \frac{\partial^2 C}{\partial z^2}, \tag{6}$$

with initial and boundary conditions

$$C(z = -\infty, t) = 0 ; \quad C(z, t = 0) = 0 ; \quad D \left. \frac{\partial C}{\partial z} \right|_{z=0} = j^S . \tag{7}$$

Here, j^S is the rate of the barrier (flip-flop) process of adsorption-desorption from the monolayer to the subsurface. For j^S, we assume the following linear phenomenological relationship holds true [6,46,47]:

$$j^S = k_d \left[C_{eq} - C(z = 0) \right] = \frac{\Gamma}{\tau_d} \left[1 - \frac{C(z = 0)}{C_{eq}} \right]. \tag{8}$$

Here, we introduced the characteristic time for desorption, τ_d (the average time a surfactant molecule spends at the surface before desorbing), related to the desorption constant k_d as

$$\tau_d = \Gamma / k_d C_{eq}; \tag{9}$$

τ_d is a parameter of transparent physical meaning which is going to be useful when we make comparison between different desorption kinetic models. The subsurface concentration $C(z = 0)$ in eqn (8) is smaller than that of the solubility C_{eq} of the monolayer because of the slow barrier processes of desorption (of rate $v_d = k_d C_{eq}$) and adsorption (of rate $v_a = k_d C(z = 0)$). The linear coefficient k_d and the characteristic time τ_d are independent of the subsurface concentration, but are unknown functions of Γ (compare to [46,35,38,39]). An immediate aim of our work is to determine experimentally τ_d as a function of Γ.

For monolayer dissolving under conditions of constant surface tension and adsorption, the solution to the problem set by eqn (6)-(8) for the flux from the surface to the bulk reads

$$j^S = k_d C_{eq}\, e^{t/\tau_{tr}} \left(1 - \mathrm{erf}\sqrt{t/\tau_{tr}}\right), \tag{10}$$

where the time τ_{tr} for transition from barrier to diffusion-controlled regime [48] stands for

$$\tau_{tr} = D / k_d^2 = \tau_d^2 D C_{eq}^2 / \Gamma^2. \tag{11}$$

In the limit of short times (thin diffusion layer, fast diffusion, barrier control), eqn (10) simplifies to a constant flux: $j^S = k_d C_{eq}$. In the other limit of long times (thick diffusion layer, diffusion control), a $t^{-1/2}$-dependence is obtained instead: $j^S = C_{eq}(D/\pi t)^{1/2}$. The change of the area of the monolayer under isobaric conditions follows from eqn (10) and the mass balance,

$$\frac{1}{A}\frac{dn}{dt} = \frac{\Gamma}{A}\frac{dA}{dt} = -j^S, \tag{12}$$

where $n = \Gamma A$ are the adsorbed moles. Upon integration of eqn (12), one obtains

$$\ln\frac{A_0}{A} = \frac{\tau_{tr}}{\tau_d}\left[e^{t/\tau_{tr}}\left(1 - \mathrm{erf}\sqrt{t/\tau_{tr}}\right) - 1 + 2\sqrt{t/\pi\tau_{tr}}\right], \tag{13}$$

This result has been derived by Baret et al. [6] for the considered problem, and before that by, *e.g.*, Munson [49], for a similar, in principle, electrochemical process. For short times, it simplifies to the linear dependence

$$\ln\frac{A_0}{A} = \frac{t}{\tau_d}. \tag{14}$$

Thus, at short times, the desorption is barrier controlled [41,48] and the linear coefficient in the desorption law in the τ_d-regime is $1/\tau_d$. For long times (D-regime), eqn (13) leads to

$$\ln\frac{A_0}{A} = \frac{2C_{eq}}{\Gamma}\sqrt{\frac{Dt}{\pi}}. \tag{15}$$

However, as t approaches a value of the order of L_{st}^2/D (~100 s for our data below), convection accelerates the process and leads to positive deviations from eqn (13) long before its limit (15) is reached.

3. Determination of the rate parameters from experimental data

The desorption kinetic equation (13) has two parameters: the average barrier desorption time τ_d and the characteristic time τ_{tr} for transition from barrier to diffusion control, eqn (11). However, we can independently determine Γ, C_{eq}, and D, which leaves τ_d as the only unknown. We will measure the first parameter, Γ, via the compression isotherm; the isotherm will be further combined with spreading pressure data to find also $\Delta_s\mu$ (sec. 3.1). The second unknown, C_{eq}, follows from eqn (5) using $\Delta_s\mu$ and data for the solubility of the alcohol (sec. 3.2). The third parameter, D, is determined independently in sec. 3.3 using NMR data. Finally, the knowledge of Γ, C_{eq} and D allows the main desorption kinetic characteristic – τ_d – to be accurately determined by comparing eqn (13) with desorption isobar data, sec. 3.4.

3.1. Spreading pressure of crystals and compression isotherms (σ_s, $\Delta_s\mu$, Γ)

1-dodecanol 98% delivered by Sigma Aldrich has been used for the laboratory work. Water was double-distilled with GFL 2001/2, Germany. We took a number of measures to avoid surface active impurities compromising the results – surface rinsing, control runs and others, described in detail previously [17]. The monolayers were formed by spreading chloroform solutions of dodecanol uniformly over the available surface of water in a Teflon Langmuir trough (580×145×4 mm^3). The total distance from the trough bottom to the surface (including the meniscus height) was ~6 mm. Experiments were performed at 10—30 °C. The temperature of the water in the trough was controlled within ±0.15 °C by a thermostat Lauda Eco Silver RE415, Germany. The temperature of the room was set equal to that in the trough using air conditioning system; only at 10 °C in the trough, the room temperature was higher (15—17 °C).

The surface tension was measured using a KSV Nima surface balance equipped with a platinum plate. We took measures to ensure complete wetting of the plate (pre-wetting and frequent cleaning of it, and others, described in ref. [17]). Before each experiment, we measured the surface tension of pure water, which is where surface impurities and incomplete wetting of the Wilhelmy plate affect the measurements the most. The technique reproduces the literature data with high accuracy (better than 0.05 mN/m), as demonstrated in Figure S11 in S2; the precision, however, is lower (±0.3 mN/m).

A. Spreading pressure. The equilibrium spreading tension σ_s of the dodecanol monolayer in contact with dodecanol crystals (or above 24.2 °C, lenses) has been measured to fix the standard state of the monolayer, see eqn (3). Reproducible values are often hard to obtain; to deal with the problems involved in the measurements of σ_s, we attempted to improve the experimental protocol we developed previously [17]. The most important steps in it are:

(i) Preliminary saturation with $C_{12}H_{25}OH$ of the substrate. This step is essential in order to stabilize the measurements by eliminating the monolayer desorption [17]. The saturated solutions were prepared by mixing fine dodecanol crystals with distilled water (typical treatment rate ~0.1 g/L) and leaving the mixture to equilibrate for 12-24 hours at the required temperature.

Using the so-obtained solution, several runs at each temperature have been performed, where each run involved:

(ii) filling the trough, and removal of the initially adsorbed material with rinsing and suction of the surface layer.

(iii) The rinsed surface of the saturated solution has been separated into two compartments by using a barrier. A small amount of fine dodecanol crystals was spread in one of the compartments, while the Wilhelmy plate was dipped into the second. The system was left in this state for 10 min, after which the barrier was removed. This procedure was designed in order to avoid attachment of crystals to the plate – with it, the crystallites are caught by the meniscus of the trough instead of by the meniscus of the plate, and their Brownian motion is slowed down by the dense monolayer. Even when we followed this protocol, such attachments occur often. Whenever we detected an attachment, we removed, rinsed thoroughly and returned the plate into the trough.

(iv) After the barrier has been removed and the two compartments of the trough were connected, the surfaces have been left to equilibrate for 10-20 min. We then did several perturbations of the system:

- perturbation of the monolayer with the barrier through series of compressions and expansions of the monolayer of different amplitude;
- detachment and attachment of the plate;
- addition of a fresh portion of dodecanol crystals.

We previously followed a procedure that involved extrapolation using an assumed asymptotic kinetics of relaxation [17], but the acceleration of the equilibration via perturbations appears to be a better method. Each run lasted for up to 3 h. 2-4 values of the spreading pressure were recorded in each run (usually one 10-20 min after each perturbation).

The results from these measurements are presented in Figure 1 (black dots). The line is a regression over the data, and gives for the spreading tension σ_s/[mN/m] = 28.9–0.14×T(°C); the standard deviation of the data off this line is ±1.0 mN/m. Within the precision of the measurement, the respective spreading pressure is independent of T and is equal to $\pi_s^S = \sigma_0 - \sigma_s$ = 46.8±1.0 mN/m.

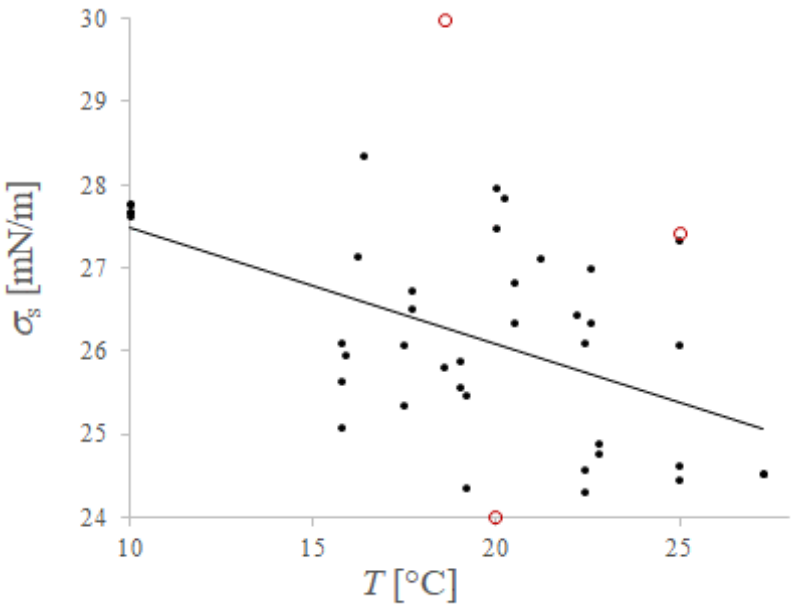

Figure 1. Spreading tension of dodecanol crystals (below 24.2 °C) and droplets (above 24.2 °C) as a function of the temperature. Solid circles: Wilhelmy plate results for surface with spread crystallites. Empty circles: bubble shape tensiometry in saturated dodecanol solution. Line: linear regression.

As a control test, we made an independent measurement of σ_s using profile analysis tensiometry in the emerging-bubble regime (PAT-1, Sinterface, Germany) for the same saturated solutions at 3 temperatures. At two of these temperatures, it took 4-5 h to saturate the surface (an example is given in Figure S12 in S3). The so-measured surface tensions of the saturated solutions are given in Figure 1 as red circles. Complete agreement with the crystal spreading pressure cannot be expected, as the crystals can alter due to diffusion of water into the crystal, *i.e.* the saturated solution is at chemical potential of the surfactant slightly lower from the one of the pure crystals. Attachment of crystals to the bubble is also possible. Despite these complications, the profile analysis tensiometry and the Wilhelmy plate yield values of σ_s in reasonable agreement with each other.

B. Compression isotherms (surface tension vs. area), and correction of the apparent area per molecule for the solubility of the monolayer. To produce the $\pi^S(A)$ isotherms, the films were compressed by means of shifting a barrier with a constant velocity, while the change of π^S with the area A of the monolayer was recorded. Since we are using a sparingly soluble surfactant, the desorption process causes a steady decrease of the total adsorbed quantity n. The output of the apparatus is *an apparent adsorption* n_0/A that is higher than the *actual* adsorption $\Gamma = n/A$, where n_0 is the initial quantity of surfactant spread on the substrate and n is the actual adsorbed quantity after a fraction of n_0 dissolves. Therefore, the measured isotherms have to be corrected for the dissolution. To do so, we previously developed a procedure where the data for isobaric desorption are used to correct the compression experiments [17]. Here, we used a conceptually

similar but significantly improved procedure, both more accurate and easier to perform, which is described in S4.

A difficult problem we experienced with the compression runs was the transport of adsorbed dodecanol through the barrier, to the free surface on the other side of the barrier. This process occurred in a random fashion: some isotherms were affected significantly, while others were not affected at all. We tried to investigate the process by placing dodecanol crystals in one compartment of the Langmuir trough, separated from a second compartment via the barrier, and measuring the surface tension in the second (Figure S20 in S5), but its random nature prevented our attempts to correct for it. The frequency of occurrence of leakages increased with the temperature and the density of the monolayer. At low temperatures (<20 °C), one out of 2-3 isotherms was affected. Therefore, we recorded 5-6 isotherms at each T; 2-3 of these were shifted to smaller areas to a random amount, and were discarded; the others agreed well and were assumed to be correct. At 23 and 25 °C, we had to do more isotherms to produce 2-3 that agree with each other. The leakages made it impossible to produce unaffected isotherms above 27 °C.

The measured isotherms are presented in Figure 2. In Figure S15 in S4, we compared them with literature results at 10 and 15 °C [50]. To facilitate the computation of $\Delta_s\mu$ through the integral (3), we used regression formulae similarly to ref. [17], but with a simplified expression:

$$\frac{1}{\Gamma} = \begin{cases} g_1 \dfrac{1 + g_2\left(1-\pi^S/\sigma_0\right)^{m_2} + g_3\left(1-\pi^S/\sigma_0\right)^{m_3}}{1-\left(1-\pi^S/\sigma_0\right)^{m_1}}, & \pi^S < \pi^S_{pt}; \\ g_4 - g_5\pi^S, & \pi^S > \pi^S_{pt}. \end{cases} \qquad (16)$$

The values of the parameters g_i & m_i of this regression are tabulated in Table 4 in S4, and are compared to the experimental data in Figure 2. As in ref. [17], we corrected for the kinetics of the liquid expanded (LE)-liquid condensed (LC) phase transition (Figure S16 in S4), related to the formation of long-lived metastable structures in the heterogeneous film [51]. The measured isotherms allow the determination of the characteristics of the LE-LC phase transition (such as heat of phase transition); these are not directly relevant to the present study, but for future reference, the analysis is provided in Figure S19 in S4.

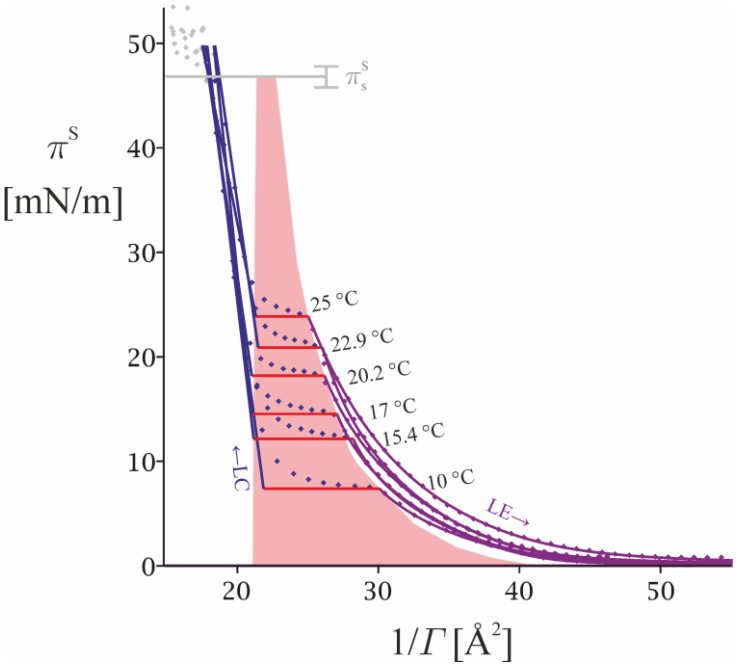

Figure 2. Surface pressure vs. area per molecule of dodecanol monolayers at various temperatures. The points are the measured π^S; the lines are regressions with eqn (16). The grey line marks the spreading pressure of the crystals, and the respective bar represents the experimental standard deviation in its value. The shaded area under the binodal corresponds to the two-phase region of the monolayer.

3.2. Solubility of dodecanol (C_s and C_{eq})

The solubility of dodecanol is very low and hard to measure. The values reported in the literature vary within two orders of magnitude (C_s = 0.02 mM at 25 °C according to ref. [52,53]; 0.2 mM from ref. [54]; 5 mM cited in ref. [55]). In our previous work [31], we attempted to determine C_s directly from the isobaric desorption data, but this approach is inaccurate, as the effect from a larger value of C_s can be effectively compensated for by proportionally larger desorption time τ_d. Here, we use instead the solubility value 0.016 mM at 25 °C reported by Yalkowsky and Valvani [56], which agrees well with the extrapolated value from the data of Hommelen [29].

We further used the known heats of dissolution of dodecanol to compute C_s at temperatures different from 25 °C. Dodecanol is liquid at 25 °C. For the heat of dissolution of the liquid $C_{12}H_{25}OH$ in water, we used the value h_s^L = 10.9 kJ/mol [57,58]. The phase transition to solid dodecanol occurs at T_m = 24.2 °C. To calculate the heat h_s^C of dissolution of the dodecanol crystals, we utilize the value of the heat of fusion of the alcohol, h_m = 40.3 kJ/mol at the melting temperature [59]: from it and Hess's law, we obtain $h_s^C = h_m + h_s^L$ = 51.2 kJ/mol. Putting these numbers together, for the solubility of dodecanol we obtain the following van 't Hoff dependence:

$$C_s(T) = \begin{cases} C_{s,m} \exp\left[-\dfrac{h_s^C}{R}\left(\dfrac{1}{T} - \dfrac{1}{T_m}\right)\right], & T < T_m; \\ C_{s,m} \exp\left[-\dfrac{h_s^L}{R}\left(\dfrac{1}{T} - \dfrac{1}{T_m}\right)\right], & T > T_m. \end{cases} \tag{17}$$

Here, C_m = 0.0158 mM is the solubility of dodecanol at the melting temperature T_m. The dependence is illustrated in Figure 3. Eqn (17) involves two approximations: for negligible heat capacity of the dissolution (constant heats h_s^C and h_s^L in the considered temperature interval), and for negligible difference of the solubility of the pure crystals and crystals saturated with water.

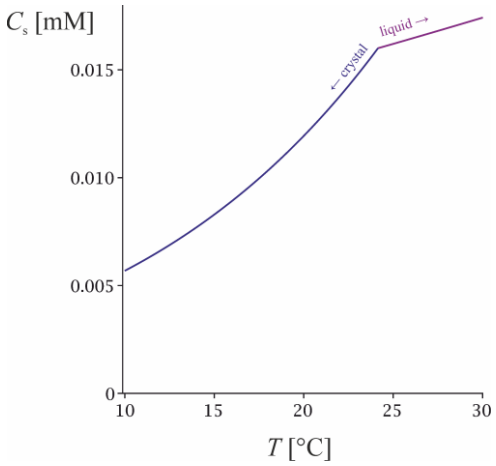

Figure 3. Solubility of $C_{12}H_{25}OH$ in water as function of temperature, eqn (17).

In view of the disagreeing reports on the values of C_s in the literature, we designed an independent test of the value from ref. [56], as follows. The potentials $\Delta_s\mu$ computed via eqn (3) from the compression isotherm at each surface pressure, together with eqn (5) for the solubility C_{eq} of the monolayer and the value of C_s = 0.0120 mM at 20.2 °C (Figure 3), allow us to deduce the surface pressure vs. concentration isotherm as done in Figure 4 (solid lines). This experimental isotherm can be compared to the sticky disc adsorption model of Ivanov et al. [45,60,61,62], known to work well for the LE phase of alcohols [60]. The equation of state of a sticky disc fluid reads:

$$\frac{\pi^S}{k_B T} = \frac{R_\beta - 1}{2\alpha\beta(1-\alpha\Gamma)}, \quad \text{where} \quad R_\beta = \sqrt{1 + 4\beta\frac{\alpha\Gamma}{1-\alpha\Gamma}}\,. \tag{18}$$

Here, α is hard-disc area of an adsorbed surfactant molecule (α = 16.5 Å^2 following from crystallographic data [45,60]) and β is lateral attraction parameter (26.4 for dodecanol, theoretical value at 21 °C, cf. *table 2* in the supplement of ref. [60]). The respective activity coefficient is given by [45]:

$$\ln\gamma^S = -\ln(1-\alpha\Gamma) + \left(2 + \frac{1}{\beta}\right)\ln\frac{2}{1+R_\beta} + \frac{\alpha\Gamma(4-3\alpha\Gamma)}{(1-\alpha\Gamma)^2}\frac{2}{1+R_\beta}\,. \tag{19}$$

Together with the theoretical adsorption constant of dodecanol, K_a = 440 μm [60], this formula defines the adsorption isotherm (4) for $C_{12}H_{25}OH$ in the LE state. The theoretical π^S vs. C_{eq} dependence following from the sticky disc model, eqn (18),(19)&(4), is compared with the one deduced from the experimental compression isotherms and the value of C_s in Figure 4. According to eqn (5), were the real value of C_s higher than 0.012 mM (as suggested in ref. [52-55]), the $\pi^S(C_{eq})$ curve deduced from our compression isotherms would shift proportionally to C_s on the right of the sticky disc model prediction. Instead, the agreement is excellent between 5 and 20 mN/m. There is discrepancy in the low-pressure region, but this is not surprising – the sticky disc model is known to fail close to the critical point of the gaseous-LE phase transition [45], and the data for dodecanol monolayer at π^S < 3-4 mN/m indeed fall into this region [45,60].

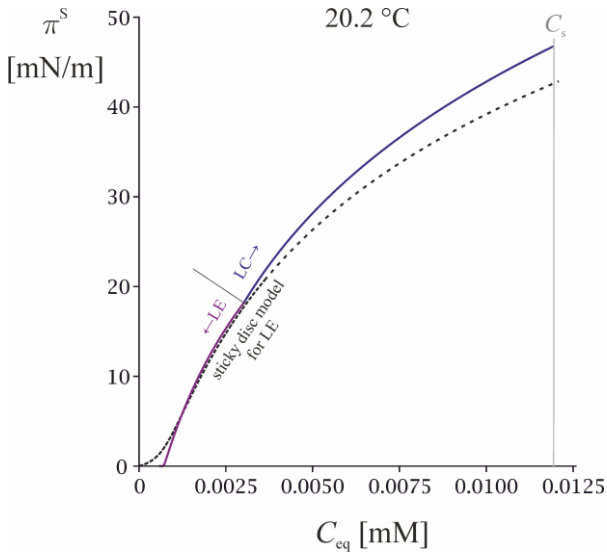

Figure 4. Equilibrium surface pressure vs. concentration isotherm. Solid lines are deduced from the compression isotherms through eqn (5)&(3), using the value 0.0120 mM for the solubility C_s of dodecanol crystals. The dashed line stands for the theoretical predictions from the sticky disc model, eqn (18)-(19). The agreement observed in the LE region is a confirmation that the value of C_s is correct.

3.3. Diffusion coefficient of alcohols in water (*D*)

Often [39,36,63], when data for adsorption kinetics are interpreted, the diffusion coefficient D is left as a free adjustable parameter determined from the data themselves. We made an attempt to do so ourselves, but found that our desorption kinetics data can be interpreted using various combinations of values of D and τ_d with similar success in terms of deviation of the model (13) from the data. Therefore, we instead determined D independently. We are not aware of a method that would allow D of $C_{12}H_{25}OH$ in water to be directly measured, due to this alcohol's extremely low solubility. We instead measured the diffusion coefficient D_{D_2O} for a few alcohols

shorter than dodecanol in heavy water, supplemented these results with literature data, and used a simple model to extrapolate to $n = 12$.

The measurements of D_{D_2O} have been performed at 20 °C using pulsed-field gradient NMR experiments. ^{1}H-NMR spectra were acquired on a Bruker Avance III HD 500 MHz spectrometer (Bruker BioSpin GmbH, Karlsruhe, Germany) with a dual ^{1}H/^{13}C cryoprobe. We used the standard Bruker pulse program, *ledbpgp2s*, employing a stimulated echo and longitudinal eddy-current delay using bipolar gradient pulses [64] with 2 spoil gradients. The diffusion coefficients D_{D_2O} were calculated by fitting the experimental data with the equation [65]:

$$I = I_0 \exp\left[-D_{D_2O}\gamma^2 g^2 \delta^2 \left(\Delta - \delta/3\right)\right]; \tag{20}$$

here, I_0 is the NMR signal intensity in the absence of any gradient, γ is the gyromagnetic ratio of ^{1}H nuclei, g is the strength of the gradient pulse of duration δ, and Δ is the observation time (the separation of the gradient pulses). The measurements were carried out holding constant $\delta = 5$ ms and $\Delta = 100$ ms, and varying the magnetic field gradient g. The NMR spectra were acquired and processed using TopSpin software (Bruker GmbH). Saturated aqueous solution of several n-alcohols (hexanol, octanol, nonanol and decanol, Sigma-Aldrich, >99% pure, GC grade) in D_2O were analysed. They were prepared by mixing an excess amount of the desired alcohol with 2 mL of D_2O in a thermostated glass vials at 20 °C for 24 hrs. The undissolved alcohol was removed from the solution by filtration through a 0.22 μm PTFE syringe filter.

The measured values of D_2O are summarized in Table 1. The solubilities of nonanol and decanol are also too low to obtain accurate diffusion coefficients with the NMR technique, and the measured D_{D_2O} for them appear to be underestimated. We attempted to measure also D_{D_2O} for saturated dodecanol using the same method, but the obtained value is definitely an artefact (an order of magnitude lower than expected). The results for D_{D_2O} in heavy water were reduced to D in normal water using the formula

$$D = D_{D_2O}\frac{\eta_{D_2O}}{\eta}, \tag{21}$$

where $\eta = 1.00$ and $\eta_{D_2O} = 1.25$ mPa·s are the respective viscosities of H_2O and D_2O at 20 °C. To reduce the value of D at $T = 293$ K to standard temperature of $T_0 = 298$ K, we used

$$D_0 = D(T)\frac{T_0\eta(T)}{T\eta_0}, \tag{22}$$

where D_0 and η_0 are the diffusion coefficient and the viscosity in water at T_0. Both equations are forms of the Einstein-Stokes relation, with the assumption that the Stokes radius of the considered alcohols is the same for H_2O and D_2O, and has no significant dependence on T. A similar assumption has been made by others [66,24]. Stilbs [67] also used NMR to determine the diffusion coefficient of hexanol in D_2O (but at 25 °C, where $\eta = 0.89$ and $\eta_{D_2O} = 1.11$ mPa·s). After correcting for the temperature dependence according to eqn (21), the result of Stilbs agrees well with ours, Figure 5.

Table 1. Diffusion coefficient of saturated solutions of alcohols in D_2O (measured) and H_2O (calculated through eqn (21)&(22)).

	$10^{10}\times D_{D_2O}$ [m^2/s] in D_2O, 20 °C (measured [a])	$10^{10}\times D$ [m^2/s] H_2O, 25 °C (corrected)
$C_6H_{13}OH$	5.8 ± 0.2	8.0
$C_8H_{17}OH$	4.48 ± 0.015	6.19
$C_9H_{19}OH$	4.02 ± 0.07	5.55
$C_{10}H_{21}OH$	3.0 ± 0.2	4.2

[a] An average of the values obtained from the proton peaks at chemical shifts 3.681, 1.327, 1.158, 1.015, and 0.738 ppm.

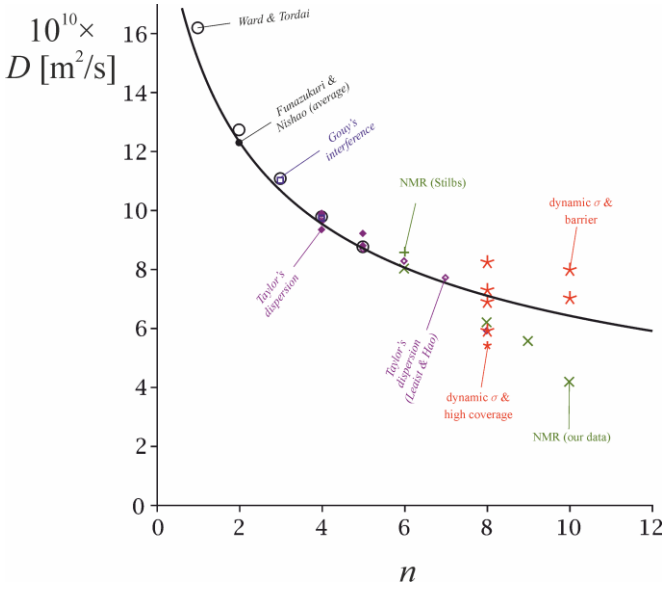

Figure 5. Diffusion coefficient of n-alkanols in water as a function of the number of carbon atoms in the chain. All data (ours and those from ref. [63,66-73,76,77,39,36]) are reduced to 25 °C and H_2O, as explained in the text. The line is the model eqn (23).

We supplemented the NMR results with D values measured with Taylor's method by Leaist and Hao [68,69] and others [70-73], and by the interference method [74,75] (reducing the data to 25 °C using eqn (22), where necessary). We utilized also the average value for ethanol from the values assembled in ref. [72], and the literature data from *fig. 2* in ref. [66]. For higher alcohols, we also collected some values of D that were obtained from the interpretation of dynamic surface tension data, but only when explicit account for the barrier of desorption has been taken [76,77,39,36]; these values are very scattered as they are sensitive to the adsorption model used by the authors, but still, they agree with the general trend of D as a function of n (Figure 5). There are many values of D reported as extracted from dynamic surface tension measurements, but with the barrier desorption rate neglected [63,21,78,79]; these are nearly

always very low compared to the general trend. The reason is that, when the flip-flop rate is ignored in an adsorption kinetic model, it can be compensated by artificial decrease of the diffusion coefficient to obtain similar dynamic surface tension curves (as noted already by Ward and Tordai [66], and analysed in detail by Liggieri et al. [80,81]). As we shall show in sec. 3.4 below, the rate of barrier desorption becomes infinite at high densities of the desorbing monolayer, and for such monolayers, the assumption for diffusion-controlled adsorption is reasonable. Unfortunately, most of the data reported in the literature refer to dilute monolayers; the only value of D we found obtained in this way with relatively dense monolayer is by Defay and Hommelen [63], for 3.44 mM octanol in water – it is also plotted in Figure 5.

To extrapolate the assembled data to dodecanol, we assumed the following scaling behaviour for D with the carbon number of the alcohols:

$$D = D_{n=0} / \sqrt{n+1}\,; \tag{23}$$

this is again a form of the Einstein-Stokes formula, with the assumption that the effective Stokes radius scales as $r_S = r_{S,n=0}\times(n + 1)^{1/2}$, typical for long unbranched molecules (we use $n + 1$ instead of n to account for the terminal OH group). We determined a best fit value of the empirical parameter $D_{n=0}$ by comparing eqn (23) with the data in Figure 5 for D of alcohols from ethanol to decanol; the obtained optimal value is $D_{n=0} = (21.3\pm1.4)\times10^{-10}$ m^2/s. With this $D_{n=0}$, eqn (23) yields $D = (5.9\pm0.4)\times10^{-10}$ m^2/s for dodecanol at 25 °C and $D = (6.4\pm0.4)\times10^{-10}$ m^2/s for decanol at 25°C. The values of D at other temperatures were calculated using again the Einstein-Stokes relation (22), in the form $D(T) = D_0 T\eta_0/T_0\eta$. The resulting numbers are summarized in Table 2 for dodecanol and Table 3 for decanol.

3.4. Desorption isobars of dodecanol (τ_d)

The main body of experiments we did was desorption isobars at several surface pressures and temperatures, where the change of the monolayer area with time was recorded at constant surface pressure. We usually did 3 desorption isobars in each run on the same substrate – one at very low surface pressure, another at medium, and a last one at high. Certainly, each next isobar is affected by the previous ones (the diffusion layer already contains surfactant at the start of the 2nd and 3rd isobar). However, the solubility of the monolayer at the lower surface pressure is 2-3 times lower than the one at the higher, *e.g.*, C_s(5 mN/m) = 0.61 μM while C_s(20 mN/m) = 1.46 μM at 10 °C, Table 2; we assumed that this is enough to make the effect small. To confirm that, we repeated several high-π^S isobars alone, and obtained similar rates of desorption. The final results suggest that some of the isobars at π^S > 30 mN/m were affected and desorbed by *ca.* 15-20% more slowly than expected. A related problem is that the desorption in the isobaric regime always have a prehistory (finite time for preparation of the monolayer and its compression to the prescribed π^S), which makes the determination of the initial moment and area inaccurate. Also, the control of π^S is imperfect: especially at low

temperatures and high surface pressures, where the monolayers are elastic, oscillations of $\pi^S(t)$ were observed, causing respective oscillations of $A(t)$, and in addition, often π^S is by 0.5-1 mN/m lower than the predefined value for the first 15-20 s of the isobar. The average π^S for the duration of the desorption isobar are reported in Table 2 (instead of the predefined one). Leakages were not frequent with the desorption isobars compared to the compression isotherms, probably due to the slower motion of the barrier; yet some have been detected, and the respective accelerated isobars were discarded.

A typical isobaric desorption curve is presented in Figure 6. It illustrates the role of the three major mechanisms of transport: barrier, pure diffusion, convective diffusion. The *pure diffusion regime*, eqn (15), predicts dissolution much faster than the experimentally observed (the *D*-curve in Figure 6); therefore, the observed rate of area decrease is impossible to explain without a desorption barrier – both pure diffusion, *D*-, and convective diffusion, C-, regimes overestimate the desorption rate. The pure *barrier transport regime*, eqn (14) and the τ_d-line in Figure 6, holds for 5-10 s (while $t << \tau_{tr}$ [48], where $\tau_{tr} \approx 50$ s from eqn (11)). The mixed barrier-diffusion regime τ_d & *D*, eqn (13) and the τ_d & *D* curve in Figure 6, is in excellent agreement with the data for the first 25 s, showing the distinctive concave shape of the A/A_0 vs. *t*, typical for diffusion process with diffusion layer of thickness $(Dt)^{1/2}$ increasing with time. Between the 25th and the 30th second, an increase of the desorption rate is observed in comparison with the τ_d & *D* curve, as the transport through the diffusion layer passes from pure diffusion to convective diffusion regime. After the 35 second, the linear C-*regime* of Ter Minassian-Saraga (or a mixed τ_d & C regime, which is also linear) is fully established.

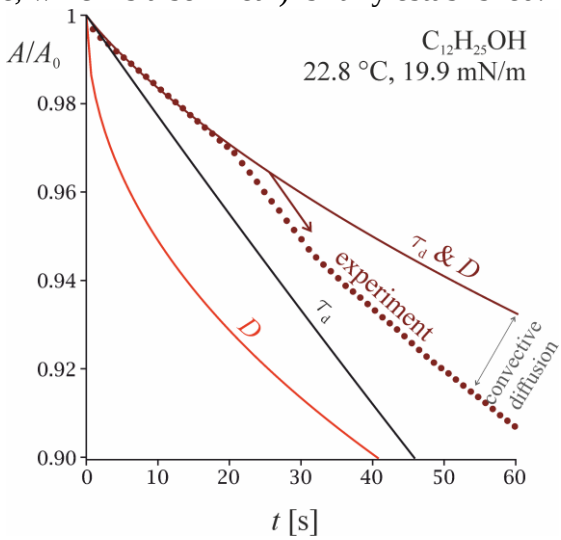

Figure 6. Desorption of dodecanol from a monolayer spread on water at π^S = 19.9 mN/m, 22.8 °C: relative monolayer area A/A_0 vs. time *t*. The desorption is under barrier control for the first 5 s – τ_d line, eqn (14). For *t* = 5—20 s, mixed barrier-diffusion regime is established – τ_d & *D* line, eqn (13). At *t* > 25 s, convection accelerates the desorption process.

The complete suppression of convection would lead to the establishment of the τ_d & *D* regime (13). In the other limit of very intensive convection (whatever the source, trough's

barrier movement, natural convection or stirring), the stagnation layer will become very thin, $L_{st} << (D\,\tau_d)^{1/2}$, which will result in purely barrier-controlled desorption following eqn (14) (an example for this behaviour will be given below). Therefore, in the presence of convection, the experimental data inevitably fall between the τ_d and the τ_d & D curves, as it is indeed observed in Figure 6 and all other isobars we analysed.

To extract τ_d, the desorption data have been analysed in 2 iterations, according to the following algorithm:

- **Iteration I**. *Step I-1:* the point where the desorption transits from τ_d & D to convective diffusion (τ_d, D & C) regime has been visually determined for each isobar. This transition often occurs with a break that is easy to identify (as in Figure 6, where it is indicated with an arrow), but sometimes it is smooth instead, and not all transition times could be accurately determined in the first iteration. *Step I-2:* the data falling in the τ_d & D regime were fitted with eqn (13), and a first-iteration values for τ_d and τ_{tr} have been determined. These were used to correct the compression isotherms, as explained in sec. 3.1B.
- **Iteration II**. *Step II-1:* the points where the transition from τ_d & D to τ_d, D & C regime occurs were corrected wherever the parameters τ_d and τ_{tr} did not agree with the general trend. *Step II-2:* the values for D from sec. 3.3 and for C_{eq} and Γ from sec. 3.1&3.2 were calculated (which involves the use of the corrected compression isotherms), Table 2. This leaves a single unknown in eqn (13): the average desorption time τ_d. *Step II-3:* all measured isobars were fitted with eqn (13) to determine τ_d. The obtained values are listed in Table 2, and Figure 7 illustrates the data at 17.1 °C, as a function of the area per molecule $1/\Gamma$.

We usually repeated iteration II to ensure that both the (τ_d & D) to (τ_d, D & C) transition point and the solubility correction of the isotherms are sufficiently accurate.

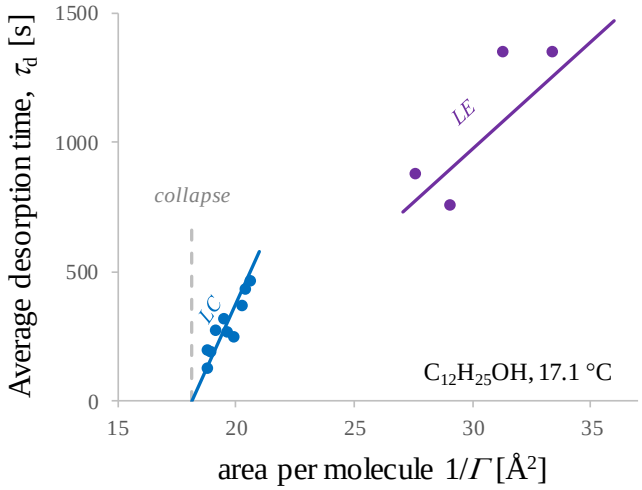

Figure 7. Average desorption time, $\tau_d = \Gamma/v_d$, vs. the area per molecule, $1/\Gamma$, of dodecanol monolayers at 17.1 °C. Lines are eqn (24), with slopes K^{LE} & K^{LC} according to eqn (25) (the values of τ_d, Γ, K^{LE} and K^{LC} are those in Table 2).

Table 2. Equilibrium and kinetic parameters for adsorption-desorption of dodecanol at various surface pressures and temperatures.

dodecanol	π^S [mN/m]	[a] $1/\Gamma$ [Å^2]	[b] C_{eq} [μM]	[c] fitted τ_d [s]	[d] final τ_d [s]	
	5.0	32.4	0.61	1710	1940	LE
T = 9.8 °C	6.8	30.5	0.71	1310	1640	
[e] $D = 3.83\times10^{-10}$ m^2/s	19.8	20.6	1.46	502	843	LC
[f] C_s = 5.5 μM	24.9	20.1	1.91	780	649	
[j] K^{LE} = 134 & K^{LC} = 331 s/Å^2	29.6	19.7	2.48	412	500	
	39.4	18.7	3.91	190	187	
	5.0	33.1	0.89	1650	1380	LE
	10.0	29.1	1.31	961	1000	
T = 15.4 °C	12.0	28.3	1.52	912	931	
[e] $D = 4.53\times10^{-10}$ m^2/s	19.9	20.5	2.31	906	526	LC
[f] C_s = 8.5 μM	29.9	19.6	3.80	675	327	
[j] K^{LE} = 92 & K^{LC} = 227 s/Å^2	34.8	19.2	4.83	495	229	
	39.7	18.7	6.11	260	134	
	3.0	36.2	0.81	2130	1480	LE
	5.0	33.3	0.97	1355	1260	
	7.0	31.2	1.13	1355	1070	
	13.0	27.6	1.75	883	772	
T = 17.1 °C	20.0	20.6	2.58	467	501	LC
[e] $D = 4.76\times10^{-10}$ m^2/s	22.9	20.4	3.01	437	449	
[f] C_s = 9.6 μM	24.9	20.2	3.32	371	418	
[j] K^{LE} = 82 & K^{LC} = 203 s/Å^2	32.9	19.6	4.95	271	295	
	34.7	19.5	5.40	320	268	
	39.8	19.1	6.89	275	193	
	42.6	18.9	7.89	193	147	
	44.6	18.7	8.64	134	117	
T = 19.9 °C	4.9	34.5	1.13	1420	1130	LE
[e] $D = 5.15\times10^{-10}$ m^2/s	10.0	29.9	1.68	761	806	
[f] C_s = 11.7 μM	29.8	19.8	5.30	229	273	LC
[j] K^{LE} = 69 & K^{LC} = 169 s/Å^2	34.7	19.2	6.73	277	187	
	5.0	34.3	1.40	942	927	LE
T = 22.8 °C	9.9	29.9	2.06	383	673	
[e] $D = 5.56\times10^{-10}$ m^2/s	14.9	27.3	2.90	338	527	
[f] C_s = 14.4 μM	24.9	20.1	5.22	170	277	LC
[j] K^{LE} = 57 & K^{LC} = 140 s/Å^2	34.5	19.0	8.29	120	126	
	4.8	36.4	1.38	615	936	LE
T = 24.8 °C	6.9	33.8	1.65	474	784	
[e] $D = 5.88\times10^{-10}$ m^2/s	9.8	31.3	2.08	459	665	
[f] C_s = 16.0 μM	15.0	28.3	3.01	259	522	
[j] K^{LE} = 51 & K^{LC} = 124 s/Å^2	24.9	21.2	5.63	152	378	LC
	30.1	20.4	7.34	117	277	
dodecanol	π^S [mN/m]	[a] $1/\Gamma$ [Å^2]	[b] C_{eq} [μM]	[c] fitted τ_d [s]	[d] final τ_d [s]	

[a] Determined from π^S through the compression isotherms in Figure 2 via the regression (16). [b] Obtained via eqn (3)&(5), with $\Delta_s\mu$ computed from the compression isotherms in Figure 2 via eqn (16) (as illustrated in Figure S17 in S4) using the spreading pressure from sec. 3.1. [c] Average desorption time obtained by fitting each desorption isobar with eqn (13) (1-parameter fit). [d] Average desorption time obtained by fitting those from column "*c*" as function of Γ and T with the model (24)&(25). [e] Diffusion coefficient as obtained in sec. 3.3. [f] Solubility C_s of dodecanol crystals/droplets as obtained in sec. 3.2. [j] Values of the linear coefficients in eqn (24) specifying the dependence of τ_d on Γ, as they follow from eqn (25) (with K_0^{LE} = 50.1 s/Å^2, E_A^{LE} = 45.3 kJ/mol, and K_0^{LC} = 122 s/Å^2 and E_A^{LC} = 45.9 kJ/mol).

It is seen in Figure 7 that, for both the LE and LC phase, the dependence of τ_d on the area per molecule is to a good approximation linear, as has been previously observed by us [31]. Another important feature of the dependence is that τ_d approaches zero as the monolayer approaches the collapse point (where $1/\Gamma$ is equal to the collapse area of the surfactant $\alpha_\perp$), *i.e.* the desorption rate from a collapsing monolayer is infinite. For alcohols, $\alpha_\perp$ = 18.2 Å^2 (as seen in Figure 2). The linear dependence in Figure 7 can therefore be written as [31]:

$$\tau_d = \begin{cases} K^{LE}\left(\Gamma^{-1} - \alpha_\perp\right) & \text{(LE region);} \\ K^{LC}\left(\Gamma^{-1} - \alpha_\perp\right) & \text{(LC region).} \end{cases} \qquad (24)$$

The desorption time τ_d can be expected to have an Arrhenius dependence on the temperature. Therefore, as $\alpha_\perp$ is nearly independent of *T*, from eqn (24) it follows that Arrhenius dependences should also hold for the linear coefficient K^{LE} and K^{LC}:

$$K^{LE} = K_0^{LE} \exp\left[\frac{E_A^{LE}}{R}\left(\frac{1}{T} - \frac{1}{T_0}\right)\right] \quad \text{and} \quad K^{LC} = K_0^{LC} \exp\left[\frac{E_A^{LC}}{R}\left(\frac{1}{T} - \frac{1}{T_0}\right)\right]. \qquad (25)$$

We used eqn (24)&(25) to fit all measured τ_d in Table 2, at all Γ and *T*, for the LE and the LC phases separately, thus obtaining the four parameters – the standard slopes, K_0^{LE} = 50±3 s/Å^2 and K_0^{LC} = 122±15 s/Å^2, and the activation energies for desorption, E_A^{LE} = 45±5 kJ/mol and E_A^{LC} = 46±10 kJ/mol (the uncertainties define the region of values of E_A and K_0 producing dispersion within 2.5% from the minimal dispersion, cf. Figure S24 in S6). The computed τ_d are listed in the last column of Table 2, and eqn (24) is illustrated for 17.1 °C in Figure 7.

The experimental $A(t)$ dependences at 17.1 °C are compared in Figure 8 with the theoretical prediction (13), with τ_d set to its "final" value following from eqn (24)&(25), and with the theoretical transition time τ_{tr} (eqn (11) with Γ, C_{eq}, and *D* from Table 2). The agreement is within the uncertainty of the experimental data. The results at 10, 15, 20, and 23 °C are similar and are shown in Figure S21 in S6. The acceleration of the dissolution process with the increase of π^S is well-represented by the model (13)&(24), as long as the mixed τ_d-*D* regime is operating. In addition, the acceleration of the desorption rate with the increase of temperature is in agreement with the Arrhenius equation (25) (cf. Table 2 and Figure S21 in S6). In most cases, the measured desorption rates at the highest surface pressures studied (30-45 mN/m) are slower than predicted by *ca.* 15%. This is most likely due to the prehistory of the respective desorption isobars: before the "initial" moment, 1-2 other isobars at lower pressures have been measured, and the monolayer has been compressed, *i.e.* the substrate is of non-zero initial concentration of surfactant, which slows down the desorption.

As time advances, the experimental desorption rate becomes faster than the one predicted by eqn (13), due to transition from pure diffusion to convective diffusion transport – wherever clear, this transition is indicated with an arrow in Figure 8, and in Figure S21 in S6. The faster the decrease of *A* with *t*, the sooner the transition to convective regime occurs, suggesting that the rate of convection correlates with the rate of desorption. This is in qualitative agreement

with the model of De Keyser and Joos [9] – according to eqn (1), the characteristic transition time L_{st}^2/D is proportional to $(\mathrm{d}\ln A/\mathrm{d}t)^{-1}$. However, we think it is more likely that the main convection source is the Marangoni flow produced by the surfactant diffusing below the trough's barrier to the monolayer-free compartment, a hypothesis we will test in the future. While natural convection alone cannot cause the observed effect, it is probably acting in combination with the Marangoni flow and the De Keyser-Joos convection.

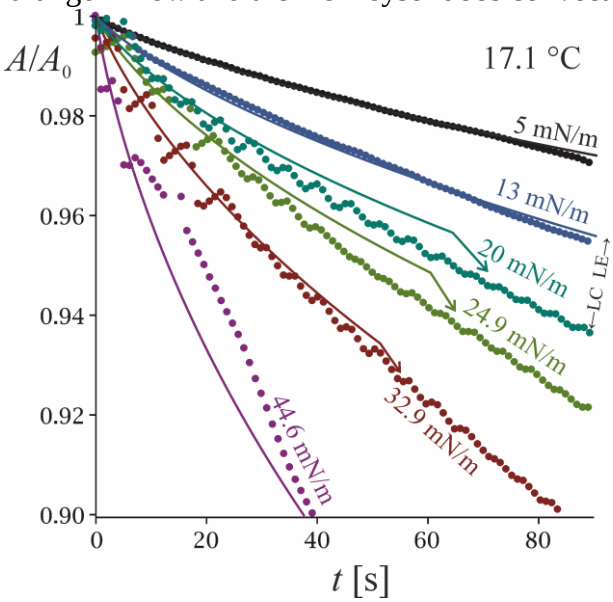

Figure 8. Desorption isobars (relative drop of the area of the monolayer vs. time) at several fixed surface pressures, 17.1 °C. At the two lowest surface pressures (5 & 13 mN/m), the dodecanol monolayer is in the LE state, the others correspond to LC phase. Lines: the theoretical prediction (13) for mixed barrier-diffusion control, with linear dependence (24) of the desorption time τ_d on $1/\Gamma$ (with K^{LE} = 82 s/Å^2 and K^{LC} = 203 s/Å^2, Table 2). The arrows indicate transition to convective regime.

At increased temperature the transition to convective regime occurs sooner, until at 25 °C (especially at pressure above 10 mN/m), the convection is so intensive that the rate of convective diffusion is much faster than the rate of the barrier process. The result is that the process follows the linear regime (14) of barrier-controlled desorption. This curious case is illustrated in Figure 9: the dashed lines stand for the τ_d-regime of desorption (eqn (14) with τ_d from eqn (24) and K^{LE} and K^{LC} from eqn (25)); the solid lines are eqn (13) of the mixed τ_d-D regime. The experimental rate suggests that the rate-determining process is the barrier desorption. This is even more pronounced at 29-30 °C, where a linear dependence of ln$A$ against t is observed for 100-200 s, in accordance to eqn (13), until most of the monolayer is dissolved (illustrated in Figure S22 in S6), with slope suggesting barrier control.

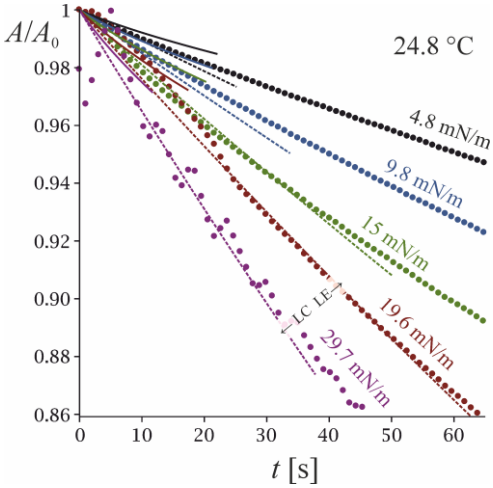

Figure 9. Desorption isobars (relative decrement of the area of the monolayer vs. time) at several fixed surface pressures and 24.8 °C. Solid lines: the theoretical prediction (13) for mixed barrier-diffusion control, with desorption time τ_d linear with $1/\Gamma$ (eqn (24) with K^{LE} = 51 s/Å^2 and K^{LC} = 124 s/Å^2, Table 2). Dashed lines: the rate of desorption under barrier control (convective diffusion much faster than the flip-flop process), according to the linear eqn (14) with the same τ_d. The data at π^S > 10 mN/m agree with pure barrier regime.

4. Discussion and conclusions

A. Comparison with literature results. De Keyser and Joos [9] reported isobars of dodecanol at 6 and 8 mN/m. Unfortunately, they did not report the temperature at which the measurements have been performed. By graphical comparison with our own data in the range 5-10 mN/m, we concluded that their temperature must have been 25 °C or slightly higher. They computed the density and the solubility of the monolayer using the Langmuir-Szyszkowski adsorption model (with parameters Γ_∞ = 7×10^{-6} mol/m^2 and a = 4.3×10^{-3} mol/m^3), which is, however, inappropriate for a surfactant as strongly cohesive as dodecanol [45] – the dangers of using an unsuitable isotherm to predict kinetics has been demonstrated by Miller et al. [34]. As a result, the values of $1/\Gamma$ computed by De Keyser and Joos are extremely high (*e.g.*, 64.4 Å^2 at 8 mN/m, instead of the correct value 32.7 Å^2 following from the isotherms in Figure 2).

De Keiser and Joos interpreted their data at long times with convective diffusion produced by the movement of the barrier and the contraction of the monolayer (with neglected barrier desorption, natural and Marangoni convection). However, in their interpretation, they used the above-mentioned erroneous values of the adsorption which are two-fold lower than the real ones. Since in their model $d\ln A/dt$ is proportional to $1/\Gamma^2$, the actual desorption rate caused by the barrier movement is 4-fold slower than what they predicted, and the agreement they reported is fortuitous. The desorption isobar which De Keyser and Joos measured at 8 mN/m is shown in Figure 23 in S6; it refers to time range of 40 min, with only 2-3 points falling in the range 0-

100 s which we investigate. Still, it is clear from Figure 23 that in the initial region, the data of De Keyser and Joos suggest complete barrier control, precisely as our data in Figure 9; only at longer times, the convective diffusion slows the process down. Therefore, the measurements from ref. [9] actually suggests very efficient natural or Marangoni convection (which the authors suspected) combined with a significant barrier for desorption.

Table 3. Equilibrium and kinetic parameters for adsorption-desorption of decanol at various surface pressures and temperatures.

decanol	π^S [mN/m]	[a] $1/\Gamma$ [Å^2]	[b] C_{eq} [μM]	[c] fitted τ_d [s]	
[d] T = 25 °C [e] $D = 6.43\times10^{-10}$ m^2/s [f] K^{LE} = 2.69 s/Å^2	5.0	49.0	15.6	86.0	LE
	10.0	32.6	25.1	38.1	
	15.0	27.6	36.1	20.9	
	20.0	25.2	49.9	14.1	

[a] Determined from the adsorption isotherm (18) with the parameters K_a = 36.25 μm and β = 20.7 obtained by comparison with surface tension vs. concentration data, Figure S25 in S7. [b] Obtained via eqn (4)&(19) from the respective value of Γ. [c] Average desorption time obtained by fitting each desorption isobar in Figure S26 in S7 with eqn (13) (1-parameter fit). [d] Baret et al. have not reported the temperature of their measurements; 25 °C is assumed by us. [e] Diffusion coefficient as obtained in Sec. 3.3. [f] Fitted value of the linear coefficient in eqn (24) specifying the dependence of τ_d on Γ.

Let us now turn to the data of Baret et al. on decanol desorption [6]. These authors correctly interpreted their results with a mixed barrier-diffusion mechanism. However, all of the physical parameters determined by Baret et al. were listed in tables that disappeared in the published version of their manuscript (*tables II-V* are cited but are non-existent). We therefore re-analysed their experimental curves for decanol in a manner similar to our results for dodecanol. To determine the density and the solubility of the decanol monolayers at each surface pressure reported in ref. [6], we used literature data for surface tension vs. concentration from ref. [29,38,39,63,82], and interpolated them with eqn (18)-(19)&(4), as described in S7. The results for Γ and C_{eq} are listed in Table 3 (Baret et al. did not report a temperature; we assumed 25 °C, based on other works by their group). The diffusion coefficient of decanol that follows from the data in Figure 5 and eqn (23) is $D_{decanol} = 6.3\times10^{-10}$ m^2/s at 25 °C. This leaves the average desorption time τ_d as the only unknown parameter in eqn (13), and we determined it for each experimental curve from ref. [6]. The comparison with the model (13) is illustrated in Figure S26 in S7, and the obtained values of τ_d are listed in Table 3. The dependence of τ_d on Γ of decanol follows with reasonable accuracy the empirical relation (24) for the LE phase, with K^{LE} = 2.69±0.14 s/Å^2. This can be compared to K^{LE} = 51 s/Å^2 for the LE phase of dodecanol at 25 °C (Table 2). According to eqn (24)&(8), at a given adsorption Γ, the ratio of the desorption rates ($v_d = \Gamma/\tau_d$) for the two alcohols is equal to the ratio of their K^{LE}-values, as $\alpha_\perp$ is the same

for decanol and dodecanol. Therefore, $C_{10}H_{21}OH$ desorbs 51 sÅ^{-2}/2.69 sÅ^{-2} = 19 times faster than $C_{12}H_{25}OH$. This means that τ_d increases by approximately a factor of $(19)^{1/2}$ = 4.35 for each CH_2 group added to the hydrocarbon chain at a given Γ in the LE region. The result can be compared with the ratio of the barrier rates of desorption of surfactants of different chain lengths from a micelle: according to Zana et al. [83], the addition of two CH_2 groups to the hydrocarbon chain of an amphiphile leads to desorption that is 10 times slower. It is noteworthy that the decanol [29] is about 17 times more soluble than dodecanol at the same temperature, confirming our previous finding [31] that the rate of barrier desorption of an amphiphile is roughly proportional to its solubility.

The order of magnitude of the values of τ_d we obtained can be compared to the one that follows from the work of Motomura et al. [18]. Similar to other authors [35,36,37,38,39,40], they postulated that $v_d = k_\Gamma \Gamma$ and $v_a = k_\Gamma \Gamma_{eq}$, *i.e.* $j^S = k_\Gamma(\Gamma - \Gamma_{eq})$, where Γ_{eq} is the adsorption corresponding to monolayer in equilibrium with $C(z = 0)$. Within the limits of validity of the linear approximation, this phenomenological relationship and our eqn (8) are equivalent (however, the form (8) leads to simpler final expression for A vs. t). The rate parameter k_Γ is related to τ_d as $\tau_d = \Gamma/v_d = 1/k_\Gamma$. Motomura et al. found for myristic acid at pH 2 and 25 °C an average desorption time of $\tau_d = 1/k_\Gamma$ = 3000 s (for Γ^{-1} in the range 30—60 Å^2), compared to ~500 s for dodecanol. Thus, the ratio of the desorption rates of $C_{13}H_{27}COOH$ and $C_{12}H_{25}OH$ is of the order of 6, in agreement with what can be expected from the lengths of their hydrocarbon chains. It is also interesting to compare our τ_d to the average time (~100 s) for a flip-flop event of an amphiphile in a bilayer [84].

The activation energies for desorption we obtained for dodecanol, E_A^{LE} = 45±5 kJ/mol and E_A^{LC} = 46±10 kJ/mol, can be compared with E_A = 62±1 kJ/mol for di(hexylglucamide), $(n\text{-}C_6H_{13})_2C[CH_2NHCO(CHOH)_4CH_2OH]_2$, as estimated by Eastoe and Dalton [24], and with the estimation ~40 kJ/mol for Triton X-100 [85,24]. Thus, the order of magnitude of this quantity also seems correct.

B. Expressions for the adsorption/desorption rates. Explicit formulae for the rate of adsorption and desorption are very useful when kinetic adsorption data for surface tension vs. time is interpreted; let us, therefore, formulate the rate expressions following from our study. Combining eqn (8),(9),(4) and the empirical eqn (24), we obtain for the LE phase the following adsorption and desorption rates:

$$v_a = \frac{\Gamma}{\tau_d}\frac{C_{z=0}}{C_{eq}} = \frac{K_a}{\gamma^S(\Gamma)K^{LE}\left(\Gamma^{-1} - \alpha_\perp\right)}C_{z=0} \quad \text{and} \quad v_d = \frac{\Gamma}{\tau_d} = \frac{\Gamma}{K^{LE}\left(\Gamma^{-1} - \alpha_\perp\right)}, \qquad (26)$$

where γ^S for short alcohols is given by eqn (19), and the adsorption constant K_a [45,60] and the kinetic parameter K^{LE} (eqn (25)) are well-defined functions of T and the hydrocarbon chain length. For longer alcohols, γ^S can be instead calculated via eqn (2)-(3) from interpolated π^S vs. $1/\Gamma$ data, like eqn (16). In this case, the following relations can be used:

$$v_a = \frac{\Gamma}{K^{LX}\left(\Gamma^{-1} - \alpha_\perp\right)} \frac{1}{C_s \exp(\Delta_s \mu / k_B T)} C_{z=0} \quad \text{and} \quad v_d = \frac{\Gamma}{K^{LX}\left(\Gamma^{-1} - \alpha_\perp\right)}, \qquad (27)$$

where K^{LX} stands either for K^{LC} or K^{LE}, depending on the surface phase in question.

The linear dependence (24) of the average desorption time τ_d on the area per molecule $1/\Gamma$ (Figure 7) can be expected to hold only within the LE and the LC regions of monolayers adsorbed at the water|air surface. Eqn (26)&(27), respectively, are not suitable for monolayers sparser than those we investigated ($1/\Gamma < 40$ Å^2). For dilute gaseous monolayer, τ_d should instead approach a constant value τ_d^G (independent of Γ) that is characteristic of a single amphiphile molecule at the neat surface (compare to the situation in, *e.g.*, ref. [86]). Consequently, another kinetic rate formula should hold true for the 2D gas:

$$v_a = \frac{\Gamma}{\tau_d^G} \frac{C_{z=0}}{C_{eq}} = \frac{K_a}{\tau_d^G} C_{z=0} \quad \text{and} \quad v_d = \frac{\Gamma}{\tau_d^G}, \qquad (28)$$

where we used that $\Gamma = K_a C_{eq}$ for infinitely dilute monolayers. Eqs (26)-(28), together with the experimental or theoretical equations of state, (16)&(3) or (19), and the rules formulated above for the dependence on T and the chain length of τ_d, define completely the phase-specific barrier adsorption-desorption rate of alcohol monolayers.

Monolayers with a structure different from that of an uncharged LE, LC or gaseous layer at water|air cannot be *a priori* assumed to follow the same adsorption-desorption rate laws (26)-(28). The cases of non-cohesive uncharged monolayers, charged monolayers, monolayers at solid surfaces *etc.* have to be studied separately.

The rate laws (24),(26)&(27) can be compared to the popular generalized Frumkin model [35-40]; its kinetic parameters a and E_d are related to the average adsorption time as $\tau_d = a^{-1}\exp(E_d/RT)$, where $E_d = constant + \nu\Gamma^n$ (many authors [87-89,32] used a variant with n = 1, *i.e.* $E_d = constant + \nu\Gamma$). The value of the constant ν is supposed to be positive; however, for $\nu > 0$, the dependence of τ_d on Γ corresponds to rate of desorption *decreasing* as the monolayer is compressed. On the contrary, our data suggests that as the collapse point is approached, the desorption rate *increases* to infinity. For many alcohols, negative values of ν have been reported (*e.g.*, *table 3* of ref. [32]), which produces a trend in agreement with our observations. In any case, all popular barrier kinetic models in the literature postulate a dependence of τ_d (or equivalently, of the desorption rate v_d) on Γ that is rather arbitrary. The approach we use instead determines a single experimental τ_d at each fixed value of Γ, and is, therefore, more straightforward.

C. Map of desorption regimes. A succinct summary of the regime transitions we observed experimentally can be made by plotting them onto a map of the desorption regimes as function of time and convection intensity. The map is constructed schematically based on the theoretical results from ref. [6,9,3,4,41,48] and is shown in Figure 10. As discussed in ref. [41,48], at vanishingly small times ($t << \tau_{tr}$, see eqn (11)), the desorption is always under barrier control.

If the convection is negligible, at $t \sim \tau_{tr}$, the mixed τ_d-D regime is acting instead, and pure diffusion control (D-regime) holds at $t >> \tau_{tr}$, Figure 10. However, as the time advances, the diffusion layer becomes thicker and, once $t \sim L_{st}^2/D$, it reaches the thickness of the stagnated layer [3,4]. The location of the stagnated layer (where $Pe \sim 1$) corresponds to a boundary between pure diffusion region near the surface and convective diffusion region far from it. From eqn (1) and the condition $L_{st} \sim (Dt)^{1/2}$, we find that the shear rate and the time for transition to convective regime are related as $dv_x/dz \sim 1/t$. Therefore, nearby the line $dv_x/dz \sim 1/t$, the desorption process will proceed under transitional diffusion regime (D & C region in Figure 10). In our experiments, this transition from pure diffusion to convective diffusion regime often occurred with a characteristic jump (the arrows in Figure 6 and Figure 8). Finally, at high enough intensity of the convection, the boundary between convective diffusion control and pure barrier control is reached, where $\tau_d \sim L_{st}^2/D$. Using that $L_{st}^2 \sim D/(dv_x/dz)$, this simplifies to $dv_x/dz \sim 1/\tau_d$ – this condition corresponds to the horizontal zone of mixed barrier-convective diffusion control (τ_d & C). At even higher shear rates, pure barrier regime is once again established. In the zone nearby the point where $dv_x/dz \sim 1/\tau_d$ and $t \sim \tau_{tr}$ simultaneously, all three factors (τ_d, D & C) contribute significantly. This schematic regime map is of general validity, independent of the source of shear, the type of the monolayer or interface.

A desorption isobar can be represented as a continuous curve on this map. For example, the succession of regime transitions observed in Figure 6 ($\tau_d \rightarrow \tau_d$,$D \rightarrow \tau_d$,C) corresponds to the lower arrow in Figure 10. All isobars observed at $T \leq 20$ °C followed a similar pattern. On the other hand, all isobars we measured at $T > 25$ °C (Figure 9, Figure S22 in S6) follow the pattern illustrated by the higher arrow in Figure 10. At 20-25 °C, the type of isobar depends on the surface pressure: the high-pressure ones are under barrier regime, while the low-pressure isobars are transient.

The regime transition temperature range we observed is close to the melting temperature T_m of dodecanol. Therefore, we investigated whether a correlation exists between the two, i.e. if more "liquidy" monolayers would desorb under barrier regime. However, the answer is negative. First, the transition range (20-25 °C for our data) must shift to lower temperatures at higher shear – according to our map, if the convection is intensive enough, all isobars will eventually proceed under barrier control irrespective of T and the fluidity of the monolayer. In addition, the decanol melts at 6.4 °C, while the regime transition temperature in the experiments of Baret et al. is above 25 °C. Therefore, the proximity between T_m and the transition temperature range for dodecanol is a fortuitous coincidence.

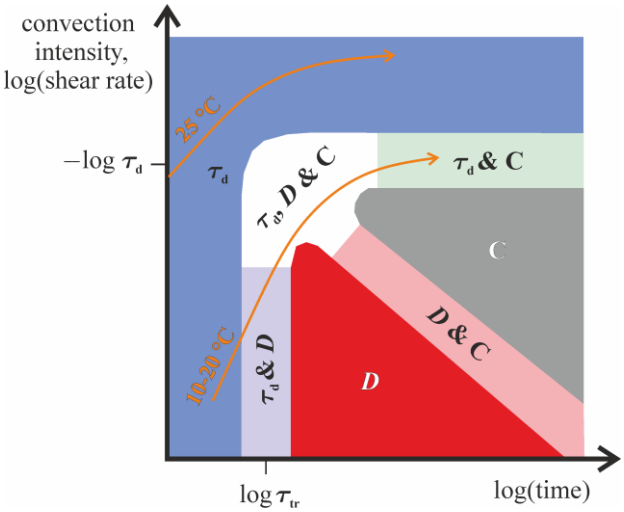

Figure 10. Map of the regimes of desorption from a flat surface against time after spreading the monolayer and convection intensity.

D. Conclusion. Let us finally summarize the most important findings of our study of the mechanism of desorption of alcohols from monolayers spread on water|air.

(i) The first important conclusion from our dodecanol data in Figure 6, Figure 8, Figure S26 in S7 *etc.* is that a significant slowdown of the desorption process occurs due to an existing adsorption/desorption barrier. It could be argued that the same data can be fitted with pure diffusion or mixed diffusion-convection mechanism if the diffusion coefficient is left as a fitting parameter. However, the resulting value of D will be dubious – by a factor of about 2 smaller than the expected one (4—6×10^{-10} m^2/s for dodecanol at 10—25 °C, sec. 3.3). Evaporation and convection cannot explain the slowdown – they can only accelerate the process compared to the pure diffusion-controlled desorption. The only plausible explanation for the decrease of the desorption rate compared to pure diffusion is, therefore, a slow rate of barrier desorption. Note, however, that the obtained values of τ_d are correct only if there is no significant contribution from evaporation and convection; it is actually possible that the values we report set only a *lower limit* for the real ones, *i.e.* it is possible that the desorption barrier process is even slower but the decrease of the area is accelerated by the simultaneous processes of convection and evaporation.

(ii) We used a combination of four experiments to determine accurately the rate of barrier desorption – the auxiliary compression isotherms, spreading pressure, and NMR measurements are used to determine Γ, C_{eq} and D, and then the desorption isobars are used for τ_d alone.

The rate of barrier desorption was experimentally analysed as a function of Γ, surfactant structure and temperature. The data show that the characteristic time for desorption (τ_d = Γ/desorption rate) decreases with the compression of the monolayer, approaching zero (infinite desorption rate) near the monolayer collapse, cf. eqn (24) and Figure 7. This allows us to give a curious kinetic definition of "collapse point" as the conditions under which the rate of flip-

flop desorption becomes infinite (thus giving a possible answer of question #1 from the list of Franses et al., "*what are the causes and events which trigger monolayer collapse?*" [90]). The dependence of τ_d on the area per molecule $1/\Gamma$ is approximately linear, eqn (24). The dependence of the rate on temperature for dodecanol follows the Arrhenius form (25) with activation energy of 45-46 kJ/mol. The addition of each CH_2 group leads to decrease of the barrier desorption rate by a factor of approximately 4.35. The order of magnitude of these values agrees with the scarce data available in the literature.

These results can be used to test different hypotheses about the molecular mechanism of the flip-flop process behind the barrier desorption process. Two particularly interesting hints are the following features of the process:

- the activation barrier is approximately independent of the density of the monolayer in the LE and LC regions (E_A^{LE} = 45.3±5 and E_A^{LC} = 45.9±10 kJ/mol);
- the rate of barrier desorption increases quickly with the length of the hydrocarbon tail, suggesting that the energy barrier rises roughly by 4 kJ/mol (1.5×*RT*) per CH_2.

Shin and Abbott [86] hypothesized tentatively that the molecular origin of the barrier is related to the dynamics of hydrophobic solvation, which seems to agree with these two features. Yet, the question remains open.

(iii) We gave experimental evidence for pure barrier control of the desorption process at high convection rates, Figure 9.

(iv) As stated in the introduction, one of our main aims in this work is to revive the desorption isobar method to study the kinetics of adsorption-desorption. The method has an important advantage over the competing techniques: the desorption is followed at constant monolayer density. The data is relatively easy to collect and simple to interpret. The method has, of course, some disadvantages. With respect to its precision, the first source of error is the low precision in the values of C_s (probably ±10%), π_s^S (±1 mN/m), and D (±7%). The second is the systematic errors in the isobars due to the prehistory of the experiment. The technique can be optimized with respect to both these issues – *e.g.*, a correction for the prehistory can be done similarly to the correction we did on the compression isotherms, S4. A limitation of the method is that only sparingly soluble monolayers can be studied with it, which restricts its applicability to surfactants of solubility of the order 10^{-4}-10^{-1} mM, in a limited temperature and surface pressure range. Yet the level of detail the method yields is unachievable with any other technique we are aware of, which more than compensates for these disadvantages.

Acknowledgements

The discussions with Dr. Javor Novev, Oxford University, helped us with the interpretation of the data falling in the convective diffusion regime. The work is funded by National Science Fund through Contract № 80-10-131 from 25.04.2018 with Sofia University.

Notes and references

Electronic supplementary information available: (S1) List of symbols. (S2) The Wilhelmy method and the surface tension of water. (S3) Measuring the spreading tension with bubble profile analysis in saturated aqueous dodecanol. (S4) Correcting the adsorption isotherms for the solubility of the dodecanol and the kinetics of the LE-LC phase transition. (S5) Leakage through the barrier. (S6) Dodecanol – additional data. (S7) Decanol data.

1. J. T. Davies and E. Rideal. Interfacial phenomena. Academic Press, 1963. Chapter 4.
2. A. W. Adamson and A. P. Gast. Physical chemistry of surfaces, 6th ed. Wiley, 1997. Sec. IV-7.
3. L. Ter Minassian-Saraga, J. Chim. Phys., 1955, 52, 181–200.
4. L. Ter Minassian-Saraga, J. Colloid Sci., 1956, 11, 398–418.
5. G. S. Patil, R. H. Matthews and D. G. Cornwell, J. Lipid Research, 1973, 14, 26–31.
6. J. F. Baret, A. G. Bois, L. Casalta, J. J. Dupin, J. L. Firpo, J. Gonella, J. P. Melinon and J. L. Rodeau, J. Colloid Interface Sci., 1975, 53, 50–60.
7. G. S. Patil, R. H. Matthews and D. G. Cornwell. Estimation of ionization in unstable fatty acid monolayers from desorption kinetics. Relationships between ionization, field strength, and cation selectivity. Advances in Chemistry, 1975, vol. **144**. Chap. 5.
8. R. D. Smith and J. C. Berg, J. Colloid Interface Sci., 1980, 74, 273–286.
9. P. De Keyser and P. Joos, J. Colloid Interface Sci., 1983, 91, 131–137.
10. F. MacRitchie, J. Colloid Interface Sci., 1985, 105, 119–123.
11. D. J. Chaiko and K. Osseo-Asare, Solvent Extraction Ion Exchange, 1987, 5, 287–299.
12. D. Vollhardt and U. Retter, J. Phys. Chem., 1991, 95, 3723–3727.
13. P. Joos and M. van Uffelen, J. Colloid Interface Sci., 1993, 155, 271–282.
14. J. P. Slotte and S. Illman, Langmuir, 1996, 12, 5664–5668.
15. N. V. Romeu, P. Dynarowicz-Łątka, J. M. Trillo, J. R. Seoane and O. C. Mouzo, J. Colloid Interface Sci., 1998, 198, 179–182.
16. D. J. Chaiko and K. Osseo-Asare, Colloid Surfaces A, 2000, 175, 335–347.
17. T. V. Peshkova, I. L. Minkov, R. Tsekov and R. I. Slavchov, Langmuir, 2016, 32, 8858–8871.
18. K. Motomura, A. Shibata, M. Nakamura and R. Matuura, J. Colloid Interface Sci., 1969, 29, 623–628.
19. A. A. Noyes and W. R. Whitney, Z. physical. Chem., 1897, 23, 689–692.
20. W. Nernst, Z. physical. Chem., 1904, 47, 52–55.
21. R. Miller and K. Lunkenheimer, Colloid Polymer Sci., 1986, 264, 357–361.
22. Y. He, P. Yazhgur, A. Salonen and D. Langevin, Adv. Colloid Interface Sci., 2015, 222, 377–384.

23. A. Casandra, B. A. Noskov, M.-Y. Hu and S.-Y. Lin, J. Colloid Interface Sci. 2018, 527, 49–56.
24. J. Eastoe and J. S. Dalton, Adv. Colloid Interface Sci. 2000, 85, 103–144.
25. C. D. Dushkin, I. B. Ivanov and P. A. Kralchevsky, Colloids Surf. 1991, 60, 235–261.
26. K. D. Danov, D. S. Valkovska and P. A. Kralchevsky, J. Colloid Interface Sci., 2002, 251, 18–25.
27. J. H. Brooks and A. E. Alexander, Proceedings of the Third International Congress of Surface Activity (Cologne), 1960, 4, 196–201.
28. J. H. Brooks and A. E. Alexander, J. Phys. Chem., 1962, 66, 1851–1853.
29. J. R. Hommelen, J. Colloid Science, 1959, 14, 385–400.
30. R. S. Hansen, J. Phys. Chem., 1960, 64, 637—664
31. R. I. Slavchov, I. L. Minkov, D. Arabadzieva and E. Mileva. Barrier desorption from sparingly soluble alkanol monolayers on water under constant surface tension. Nanoscience & Nanotechnology: Nanostructured materials application and innovation transfer, 2018, issue 18.
32. C.-H. Chang and E. I. Franses, Colloid Surf., 1995, 100, 1–45.
33. S. Dukhin, G. Kretzschmar and R. Miller. Dynamics of adsorption at liquid interfaces. Theory, experiment, application. Elsevier, 1995, Amsterdam.
34. R. Miller, E. V. Aksenenko and V. B. Fainerman, Adv. Colloid Interface Sci., 2017, 247, 115–129.
35. S.-Y. Lin, K. McKeigue and C. Maldarelli, AIChE J., 1990, 36, 1785–1795.
36. D. O. Johnson and K. J. Stebe, J. Colloid Interface Sci., 1996, 182, 526–538.
37. R. Miller, A. V. Makievski and V. B. Fainerman. In: V. B. Fainerman, D. Möbius and R. Miller, eds. Surfactants - chemistry, interfacial properties, applications. Elsevier, 2001, Chapter 4.
38. S.-Y. Lin, K. McKeigue and C. Maldarelli, Langmuir, 1991, 7, 1055–1066.
39. S.-Y. Lin, T.-L. Lu and W.-B. Hwang, Langmuir, 1995, 11, 555–562.
40. P. N. Pan, J. Green and C. Maldarelli, J. Colloid Interface Sci., 1998, 205, 213–230.
41. T. D. Gurkov, Colloid Polym. Sci., 2011, 289, 1905–1915.
42. A. I. Rusanov and V.A. Prokhorov. Interfacial tensiometry. Elsevier, 1996. Sec. 14.
43. A. Frumkin and A. Pankratov, Acta Physicochim. URSS 1939, 10, 55−64.
44. R. I. Slavchov, I. M. Dimitrova and I. B. Ivanov. Cohesive and non-cohesive adsorption of surfactants at liquid interfaces. In: R. G. Rubio, Y. S. Ryazantsev, V. M. Starov, G. X. Huang, A. P. Chetverikov, P. Arena, A. A. Nepomnyashchy, A. Ferrús and E. G. Morozov, eds. Without bounds: a scientific canvas of nonlinearity and complex dynamics. Springer-Verlag, 2013.
45. R. I. Slavchov and I. B. Ivanov, Soft matter, 2017, 13, 8829–8848.
46. R. P. Borwankar and D. T. Wasan, Chem. Eng. Sci., 1983, 38, 1637–1649.

47. Z. Adamczyk, J. Colloid Interface Sci. 1987, 120, 477–485.
48. S. N. Moorkanikkara and D. Blankschtein, J. Colloid Interface Sci., 2006, 296, 442–457.
49. R. A. Munson, J. Phys. Chem., 1962, 66, 727–729.
50. V. B. Fainerman, R. Miller, E. V. Aksenenko and A. V. Makievski. In: V. B. Fainerman, D. Möbius and R. Miller, eds. Surfactants - chemistry, interfacial properties, applications. Elsevier, 2001, Chapter 3.
51. H. M. McConnell, Ann. Rev. Phys. Chem. 1991, 42, 171–195.
52. ICSC database, www.ilo.org/dyn/icsc, October 2017.
53. C. C. Addison and S. K. Hutchinson, J. Chem. Soc. 1949, 3387–3395.
54. C. L. Yaws, J. R. Hopper, S. D. Sheth, M. Han and R. W. Pike, Waste Management, 1997, 17, 541–547.
55. Chemical Book, http://www.chemicalbook.com, October 2017.
56. S. H. Yalkowsky, S. C. Valvani, J. Pharm. Sci., 1980, 69, 912–922.
57. L. Benjamin, J. Phys. Chem., 1964, 68, 3575–3581.
58. M. H. Abraham, J. Chem. Soc., Faraday Trans. 1, 1984, 80, 153–181.
59. J. C. van Miltenburg, G. J. K. van den Berg and M. Ramirez, J. Chem. Eng. Data, 2003, 48, 36–43.
60. R. I. Slavchov and I. B. Ivanov, J. Colloid Interface Sci. 2018, 532, 746–757.
61. T. D. Gurkov and I. B. Ivanov. In Proc. 4th World Congress on Emulsions, Lyon, 2006, p. 509.
62. I. B. Ivanov, K. D. Danov, D. Dimitrova, M. Boyanov, K.P. Ananthapadmanabhan and A. Lips, Colloids Surfaces A, 2010, 354, 118–133.
63. R. Defay and J. R. Hommelen, J. Colloid Sci., 1959, 14, 411–418.
64. D. H. Wu, A. D. Chen and C. S. Johnson, J. Magnetic Resonance A 1995, 115, 260–264.
65. E. O. Stejskal and J. E. Tanner, J. Chem. Phys. 1965, 42, 288–292.
66. A. F. H. Ward, L. Tordai, J. Chem. Phys. 1946, 14, 453–461.
67. P. Stilbs, J. Colloid Interface Sci. 1982, 87, 385–394.
68. D. G. Leaist, J. Solution Chem., 1991, 20, 175–186.
69. L. Hao and D. G. Leaist, J. Chem. Eng. Data, 1996, 41, 210–213.
70. T. Tominaga and S. Matsumoto, J. Chem. Eng. Data, 1990, 35, 45–47.
71. T. Tominaga, S. Yamamoto and J.-I. Takanaka, J. Chem. Soc., Faraday Trans. 1, 1984, 80, 941–947.
72. T. Funazukuri and M. Nishio, J. Chem. Eng. Data 1999, 44, 73–76.
73. S. F. Y. Li and H. M. Ong, J. Chem. Eng. Data, 1990, 35, 136–137.
74. S. Rehfeldt and J. Stichlmair, Fluid Phase Equilibria, 2010, 290, 1–14.
75. P. A. Lyons and C. L. Sandquist, J. Am. Chem. Soc., 1953, 75, 3896–3899.

76. K. Kinoshita, E. Parra and D. Needham, J. Colloid Interface Sci., 2017, 488, 166–179.
77. S.-Y. Lin, W.-J. Wang and C.-T. Hsu, Langmuir 1997, 13, 6211–6218.
78. G. Bleys and P. Joos, J. Phys. Chem. 1985, 89, 1027–1032.
79. C. M. Phan, Can. J. Chem. Eng. 2010, 88, 688–692.
80. F. Ravera, L. Liggieri and A. Steinchen, J. Colloid Interface Sci. 1993, 156, 109–116.
81. L. Liggieri, F. Ravera and A. Passerone, Colloid Surf. A 1996, 114, 351–359.
82. S.-Y. Lin, Y.-C. Lee, M.-W. Yang and H.-S. Liu, Langmuir, 2003, 19, 3164–3171.
83. J. Lang and R. Zana. Chemical relaxation methods. In: R. Zana R, ed. Surfactant Solutions. Marcel Dekker, 1987, New York, 405–452.
84. R. I. Slavchov, T. Nomura, B. Martinac, M. Sokabe and F. Sachs, J. Phys. Chem. B 2014, 118, 12660–12672.
85. R. Miller, V. B. Fainerman, K.-H. Schano, A. Hofmann and W. Heyer, Tenside Sur. Det., 1997, 34, 357–363.
86. J.Y. Shin and N.L. Abbott, Langmuir, 2001, 17, 8434–8443.
87. V. B. Fainerman, Colloid J. USSR, 1977, 39, 91–96.
88. C.-H. Chang and E.I. Franses, Colloids Surf., 1992, 69, 189–201.
89. C. A. MacLeod and C. J. Radke, J. Colloid Interface Sci., 1994, 166, 73–88.
90. E. I. Franses, C.-H. Chang, J. B. Chung, K. C. McGinnis, S. Y. Park, and D. J. Ahn. Dynamic adsorption and tension of spread or adsorbed monolayers at the air-water interface. In: D. O. Shah, ed. Micelles, microemulsions and monolayers. Marcel Dekker, 1998. Ch. 18, sec. vii.

Barrier kinetics of adsorption-desorption of alcohol monolayers on water under constant surface tension

(supplementary information)

Ivan L. Minkov,[a,b] Dimitrinka Arabadzhieva,[c] Ibrahim E. Salama,[d,e]
Elena Mileva,[c] Radomir I. Slavchov*[,f,g]

[a] *Department of Physical Chemistry, Faculty of Chemistry and Pharmacy, Sofia University, 1 J. Bourchier Blvd., 1164 Sofia, Bulgaria*
[b] *Department of Chemistry, Biochemistry, Physiology, and Pathophysiology, Faculty of Medicine, Sofia University, 1 Koziak Str., 1407 Sofia, Bulgaria*
[c] *Bulgarian Academy of Science, Akad. G. Bonchev Str., bl.11, 1113 Sofia, Bulgaria, Sofia, Bulgaria*
[d] *Department of Chemisty, Cambridge University, CB2 1EW Cambridge, United Kingdom*
[e] *BP Institute, Cambridge University, Bullard Laboratories, Madingley Road, CB3 0EZ Cambridge, United Kingdom*
[f] *Department of Chemical Engineering and Biotechnology, Cambridge University, Philippa Fawcett Drive, West Site, CB3 0AS Cambridge, United Kingdom*
[g] *School of Engineering and Materials Science, Queen Mary University of London, Mile End Road, London E1 4NS, United Kingdom*
**E-mail: ris26@cam.ac.uk*

S1. List of symbols

A	area covered by the monolayer
A_0	area covered by the monolayer in the initial moment
C	concentration of the surfactant
$C(z = 0)$	subsurface surfactant concentration (right next to the surface)
C_{eq}	equilibrium surfactant concentration with respect to monolayer, $C_{eq} = \gamma^S \Gamma / K_a$
C_s	solubility of surfactant crystals
D	diffusion coefficient of the surfactant
j^S	rate of the (monolayer)→(subsurface) barrier process of desorption, $j^S = v_d - v_a$
K^{LC}	the empirical coefficient in eqn (24) for τ_d vs. Γ^{-1} in the LC phase
K^{LE}	the empirical coefficient in eqn (24) for τ_d vs. Γ^{-1} in the LE phase
K_a	adsorption constant of the surfactant
k_B	Boltzmann constant
k_d	rate constant for desorption, $v_d = k_d C_{eq}$
k_Γ	rate constant for desorption of Motomura et al., $v_d = k_\Gamma \Gamma$
n	amount of surfactant in the monolayer [mol]

T temperature

t time

t_{max} experimental time for transition to convective diffusion regime

v_a adsorption rate, $v_a = k_d C(z = 0)$

v_d desorption rate, $v_d = k_d C_{eq}$

z cartesian coordinate normal to the surface

α hard disc area of an adsorbed surfactant molecule ($\alpha = 16.5$ Å^2 for alcohols)

$\alpha_\perp$ crystallographic/collapse area, $\alpha_\perp = 1.1\alpha = 18.2$ Å^2 for alcohols

β lateral attraction parameter

Γ adsorption of the surfactant

γ^S surface activity coefficient of the surfactant

μ chemical potential of the surfactant monolayer

μ_0 standard chemical potential

μ_s chemical potential of the surfactant crystal

$\Delta_s\mu$ $= \mu - \mu_s$

π^S surface pressure, $\pi^S = \sigma_0 - \sigma$

σ surface tension

σ_0 surface tension of the neat surface of the solution

σ_s the value of σ for the crystal's spread monolayer

$\tau_d = \Gamma/k_d C_{eq}$, characteristic time for desorption

$\tau_{tr} = D/k_d^2$, characteristic time for transition from barrier to diffusion controlled regime

S2. The Wilhelmy method and the surface tension of water

To determine the surface tension, we measured the weight of a 19.53 mm wide platinum plate attached at the studied surface. As all techniques for surface tension measurement, the combined Langmuir trough/Wilhelmy plate method is not straightforward to use and requires special measures to be taken against artefacts. The main problems associated with it are

(i) fouling with surface active impurities has to be avoided;

(ii) complete wetting of the plate is required;

(iii) the location of the plate with respect to the surface has to be fixed (slow evaporation can lead to a decrease of the water level, and fast barrier movement can increase the water level, affecting the results);

(iv) a number of dynamic effects (kinetics of adsorption and desorption; natural convection and convection due to the movement of the barrier; leakage of surfactant through the barrier; evaporation of the water, the surfactant, and the organic solvent in which the surfactant is

dissolved upon spreading; deboarding, collapse and slow kinetics of phase transitions in the monolayer) have to be considered when the data is interpreted;

(v) in the case where the spreading pressure of crystals is measured, crystals often attach to the plate and alter the signal.

Details on the procedures that we use against these artefacts as a standard in our laboratory are given in ref. [17] (surface rinsing, cleaning and prewetting of the plate *etc.*). With regard to (i) and (ii), pure water is the worst-case scenario: in the presence of a dense monolayer of the studied surfactant, impurities affect little the state of the surface, and the wetting is significantly improved. Therefore, we measured the surface tension σ_0 of pure water before each experiment. The measured σ_0 are shown in Figure S11 as a function of T. The line is a linear regression over the data, and gives σ_0/[mN/m] = 75.64-0.138T(°C), in excellent agreement with the accepted literature values. However, the standard deviation is significant: 0.3 mN/m.

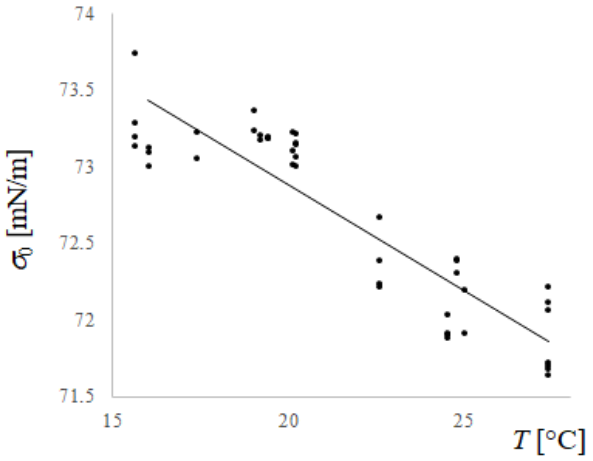

Figure S11. Surface tension of water.

S3. Measuring the spreading tension with bubble profile analysis in saturated aqueous dodecanol

For the measurements with bubble profile analysis tensiometer we used the same saturated dodecanol solutions as for experiments with the Langmuir trough. The work area of the apparatus is set to the required temperature by a thermostat. A quartz crystal cuvette is filled with 25 mL solution, saturated at the desired temperature. The cuvette is then covered with a top through which a glass capillary is fitted and dipped into the solution. An air bubble with a fixed area is formed at the tip of the capillary end and then the experiment is started. The apparatus is recording the surface tension variation with time, caused by dodecanol adsorption. During the experiment the surface area of the bubble is kept constant. The duration of the experiments was 4-6 hours, and continued until the surface tension vs. *t* curve reaches a plateau value.

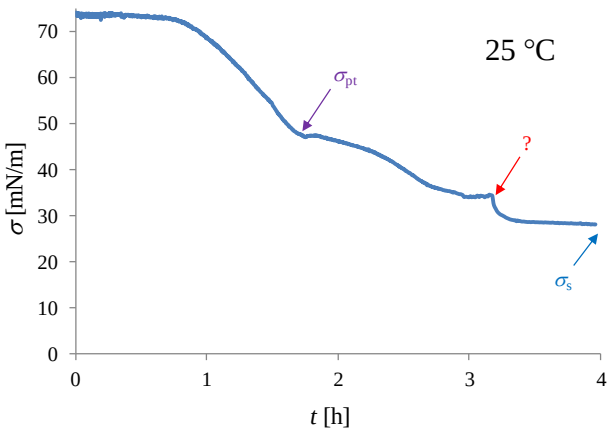

Figure S12. Dynamic surface tension of a bubble in saturated $C_{12}H_{25}OH$ solution at 25 °C.

The first kink in Figure S12 (the small plateau portion indicated with σ_{pt}) corresponds to the LE-LC phase transition. We are unsure what could be the reason the second kink (marked with "?") – we observed the same feature at 17 °C. No similar feature is observed at this particular surface tension in the σ vs. $1/\Gamma$ isotherm, see Figure 2. The shape of it suggests a sudden increase in the rate of the adsorption, which might correspond to a convection transition similar to those occurring in the isobaric desorption experiments (the arrow in Figure 6). The curve reaches a plateau after 4 h, corresponding to saturation of the surface and to value of σ equal to the spreading tension of crystals (σ_s in the Figure S12).

S4. Correcting the adsorption isotherms for the solubility of the dodecanol and the kinetics of the LE-LC phase transition

We compressed the monolayer as quickly as possible to minimize the losses due to dissolution (a compression run takes less than a minute). This option has a price – the monolayer needs some time to relax to its equilibrium state, especially in the region where the phase transitions gas-LE and LE-LC occur. If the compression is fast enough, we can approximately assume that the desorption is under barrier control. In this case, the flux of surfactant out of the surface is given by $j^S = k_d C_{eq} = \Gamma / \tau_d$ and the mass balance of the surface is given by the equation

$$\frac{1}{A}\frac{\mathrm{d}n}{\mathrm{d}t} = -\frac{\Gamma}{\tau_d}, \qquad (1)$$

compare to eqn (12). This equation is valid for both the isobaric runs and the normal compressions. For the isobaric regime of the Langmuir balance, where the adsorption Γ is constant, eqn (1) leads to

$$\frac{1}{A}\frac{\mathrm{d}A}{\mathrm{d}t} = -\frac{1}{\tau_d}, \quad \text{and} \quad \ln\frac{A}{A_0} = -\frac{t}{\tau_d}, \qquad (2)$$

i.e. eqn (14).

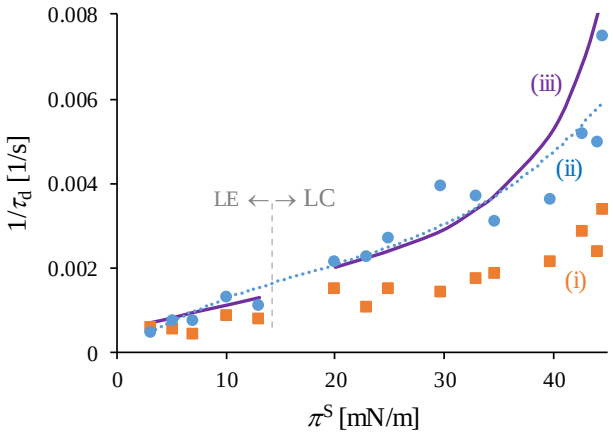

Figure S13. Reciprocal desorption time $1/\tau_d$ as a function of the surface pressure: results from isobaric desorption experiments at 17 °C. Orange squares: 1st iteration (2-parametric fits with eqn (13)). Blue circles: 2nd iteration (1-parametric fits with eqn (13)). Blue dot line: polynomial regression with eqn (3). Solid line: last iteration, eqn (24)&(16).

For every temperature and every surface pressure value, we fitted the isobaric data with eqn (13), as a first iteration, in order to determine both τ_d and τ_{tr}. The results are not very accurate, but still good enough for the correction. The data for $1/\tau_d$ as function of π^S are given in Figure S13 (orange squares). The results were interpolated using the regression formula:

$$\frac{1}{\tau_d} = c_1\pi^S + c_2\left(\pi^S\right)^2 + c_3\left(\pi^S\right)^3 \ldots \qquad (3)$$

We found that a quadratic or cubic polynomial is sufficient for the regression. The desorption time τ_d is assumed to tend to infinity when $\pi^S = 0$ (infinitely dilute monolayer); therefore, eqn (3) has no constant term.

With τ_d known, we can proceed to the integration of the kinetic equation (1) for the normal compression run to obtain the dependence of the total adsorbed quantity on time, $n(t)$. We multiply both sides of eqn (1) by $\Gamma^{-1}\mathrm{d}t$, and use that $n/A = \Gamma$:

$$\frac{\mathrm{d}n}{n} = -\frac{\mathrm{d}t}{\tau_d}. \qquad (4)$$

Integration yields:

$$\ln\frac{n}{n_0} = -J\,, \qquad \text{where } J = \int_0^t \tau_d^{-1}\mathrm{d}t\,. \qquad (5)$$

The integral J can be computed at each time step of the compression run using the following recurrent formulation of the Newton trapezium method:

$$J_1 = t_1\tau_{d,1}^{-1}/2\,; \quad J_{i+1} = J_i + \left(t_{i+1} - t_i\right)\left(\tau_{d,i+1}^{-1} + \tau_{d,i}^{-1}\right)/2\,; \qquad (6)$$

here, $\tau_{d,i} = \tau_d(\pi_i^S)$, as given by the interpolation (3), and π_i^S is the surface pressure measured at time t_i. Once J_i is known, we use eqn (5) in the form

$$\Gamma = \frac{n}{n_0}\Gamma_{app} = \Gamma_{app}\exp(-J)\,. \qquad (7)$$

In all cases, we did one or two iterations by using the results from Sec. 3.4 for τ_d, *i.e.*

(i) we used the first iteration for Γ from eqn (7) to compute the solubility of the monolayer used in Sec. 3.4 to deal with the isobaric data and calculate the second iteration for τ_d (the first being the one obtained from the 2-parameter fit, orange squares in Figure S13, and the second being the blue circles).

(ii) We used the second iteration for τ_d to compute a new interpolation according to eqn (3), and use this interpolation in eqn (5) to produce a second iteration for *J*.

(iii) The new *J* has been used to produce a second iteration for Γ via eqn (7).

The improvement from the iterations after the first was insignificant, even though the difference between the τ_d in Figure S13 and the more accurate ones obtained in Sec. 3.4 is often large in the LC region.

Our previous procedure for solubility correction has been tested in ref. [17] by comparing the results from monolayer compression at different rates of motion of the barrier of the trough. We did a similar test with the new procedure. Two compression runs of dodecanol monolayer at 25 °C were performed, one at the highest possible velocity of the barrier, 270 mm/min, and the other at a 3-fold lower speed of 90 mm/min. The results before and after the correction are illustrated in Figure S14. Before the correction, the slow isotherm is visibly shifted towards lower areas. After the correction, the two are in reasonable agreement, which proves the usefulness of the procedure. For the higher velocity, the correction leads to actual areas per molecule by 1-2 Å^2 larger than the apparent areas (and less for lower temperatures). The figure also gives an idea of how bad the assumption for desorption under barrier control is: the slight misfit of the two curves is because of the overcorrection of the slower isotherm (where diffusion slows down the process additionally, which is not accounted for in the correction procedure). As seen, the difference is small enough to ignore (smaller than the reproducibility of the isotherms).

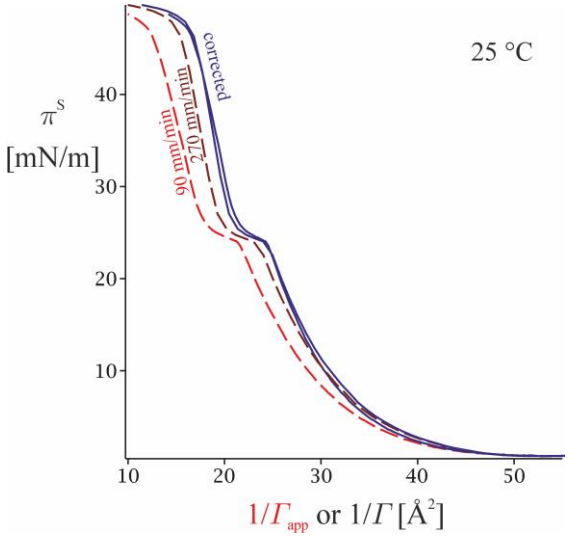

Figure S14. Surface tension vs. apparent area and corrected area per molecule of dodecanol spread on water at 25 °C: data for two barrier velocities, 90 and 270 mm/min. The dashed lines are before the correction.

Our dodecanol isotherms can be compared with those of Fainerman et al. [50] at 10 and 15 °C. Especially at 15 °C, their results are shifted towards higher densities (Figure S15); the LC region is approaching unrealistic areas smaller than the crystallographic area of solid alkanes ($1/\Gamma < 18.2$ Å^2). This means that the data from [50] are significantly affected by solubility as well. In addition, the LE-LC phase transition of Fainerman et al. is at slightly higher surface pressure than ours. This can be explained either by the presence of impurities in theirs or our dodecanol, or by imperfect thermostating (the temperatures of Fainerman et al. appear to have been by ~2° higher than ours).

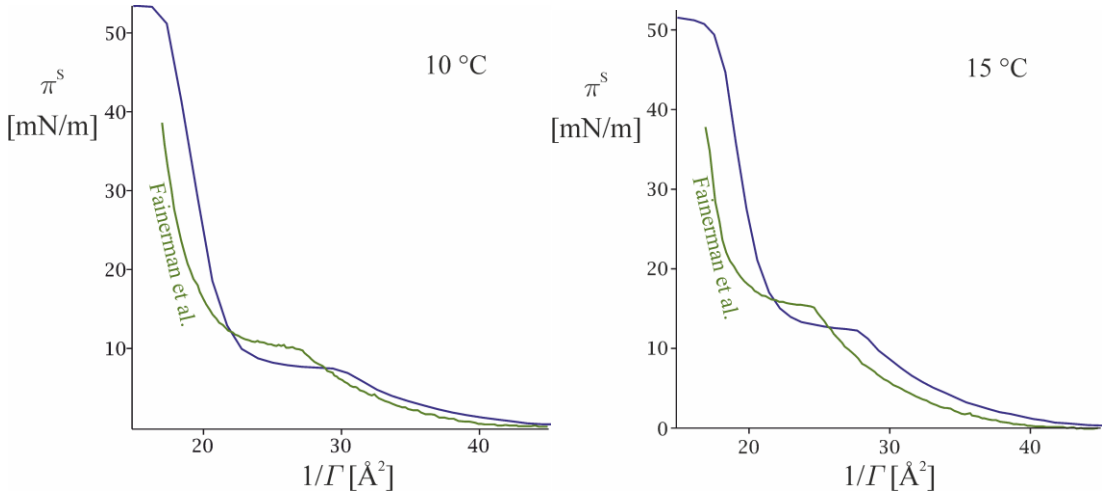

Figure S15. Comparison between our isotherms at 10 and 15 °C and those by Fainerman et al. [50].

Kinetics of the LE-LC phase transition. Since we compress the monolayer quickly, we have to correct for the increased dynamic surface pressure in the phase transition region. Once the LC domains are formed, they start to interact repulsively with each other [51], and the force applied by the barrier on the heterogeneous monolayer is partly acting against this repulsive force (similar effects are common in the three dimensional liquid-solid phase transitions, when the fractal net of solid crystals in touch with each other start to have an elastic answer against the external force). The LC region covers a very short range of areas, and we usually have only 5-6 points in this region; the first few of them are affected by the dynamics of the phase transition, and the last few are affected by the collapse. In view of these complications, we decided that the crudest approximation for the equilibrium shape of the LC region – a line – is good enough. The following procedure was applied to all data:

(i) Identify the point at which the phase transition starts (indicated with an arrow in Figure S16); the data right of this point corresponds to homogeneous LE phase, while the data left of

it refers to a heterogeneous surface with LC domains dispersed in an LE film (probably, the system relaxes to homogeneous LC monolayer eventually, but it is very likely that the LC domains and the two-dimensional LE films between them will survive even at significant compressions, close to the collapse).

(ii) The data in the LE region are fitted with eqn (16) ($\pi^S > \pi^S_{pt}$) – let the respective function be $f^{LE}(\pi^S)$. The data for the heterogeneous monolayer is fitted with a polynomial (of degree 3 or 4); we call the respective function $f^{het}(\pi^S)$.

(iii) The point at which $f^{LE}(\pi^S) = f^{het}(\pi^S)$ identifies the phase transition pressure tension π^S_{pt} and the respective equilibrium LE adsorption Γ^{LE}.

(iv) The data for the heterogeneous monolayer has an inflection. The tangent line through the inflection point of f^{het} is constructed and is assumed to represent the equilibrium state of the LC monolayer (the equilibrium LC line in Figure S16).

(v) The point of cross-section of the equilibrium LC line and the horizontal line $\pi^S = \pi^S_{pt}$ defines the area of the LC monolayer in equilibrium with the LE film.

(vi) The value of the equilibrium spreading pressure π^S_{pt} is substituted in the equation for the equilibrium LC line; this yields the area of the equilibrium spread layer.

This procedure is illustrated in detail in Figure S16, and also in Figure 2, in less detail. The edges of the horizontal dashed lines are part of the binodal for the LE-LC transition. It is remarkable that the slope of the LC region in Figure 2 (*right*) does not depend on the temperature significantly. The parameters of eqn (16) obtained via this procedure are summarized in Table 4.

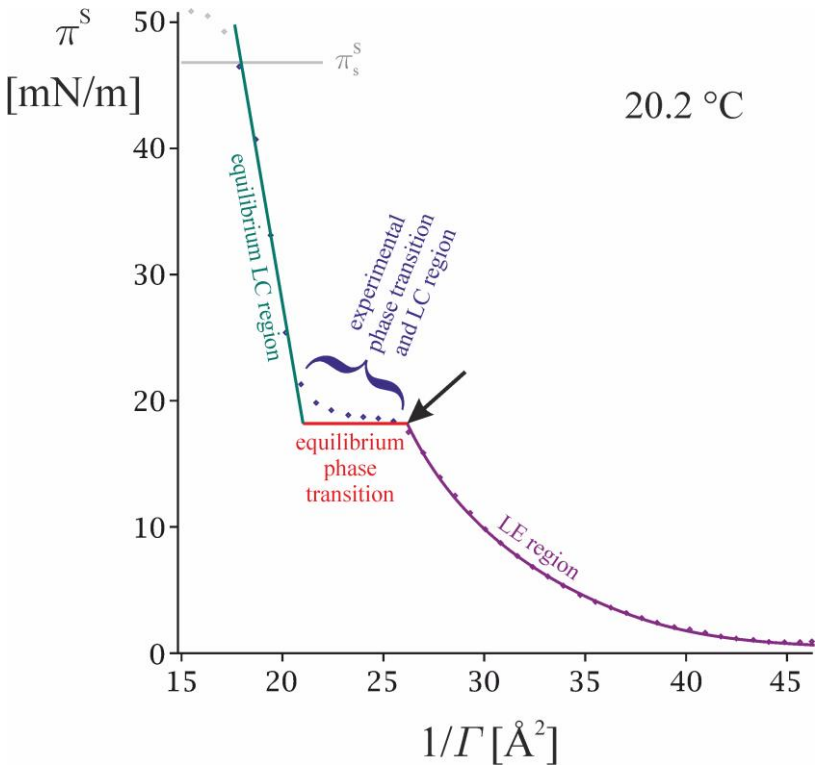

Figure S16. Correction for the kinetic effects during the LC-LE phase transition. The significant repulsion between the LC domains formed during the phase transition leads to a kinetic increase of the surface pressure π^S. The observed π^S vs. Γ^{-1} curve in this region is therefore below the theoretically expected horizontal line for a first order phase transition.

Table 4. Parameters of the equation of state (16), as obtained from the corrected π^S vs. $1/\Gamma$ isotherms.

T	**10 °C**	**15.4 °C**	**17 °C**	**20.2 °C**	**22.9 °C**	**25 °C**
g_1 [Å^2]	24.2836	30.4535	31.4014	22.2778	23.07556	14.2358
g_2	-0.0269519	-0.238060	-0.238816	-0.134695	-0.121569	-0.0585756
g_3	-0.972393	-0.758748	-0.755349	-0.859611	-0.872810	-0.934531
m_1	1	5	4	2	2	1
m_2	30	19	15	14	14	19
m_3	1	3	2	2	2	2
g_4 [Å^2]	22.5770	22.2171	22.1276	22.9717	23.6772	24.8072
g_5 [Å^{2}m/mN]	0.0978461	0.0875110	0.0762142	0.107170	0.105664	0.146501
π^S_{pt} [mN/m]	7.38686	12.1554	14.5308	18.1982	20.8908	23.8605
a^{LE}_{pt} [Å^2]	30.07	28.2120	27.0654	26.1812	26.0406	25.0290
a^{LC}_{pt} [Å^2]	21.85	21.1534	21.0201	21.0214	21.4697	21.3116
$a_{collapse}$ [Å^2]	18.00	18.12	18.56	17.96	18.73	17.9492

Figure S17 illustrates the computation via the Gibbs equation (3) of the chemical potential $\Delta_s\mu = \mu - \mu_s$ from the isotherm fits just discussed. The state of the surfactant in the crystal is used as a standard state – the integration starts at the spreading pressure of dodecanol crystals.

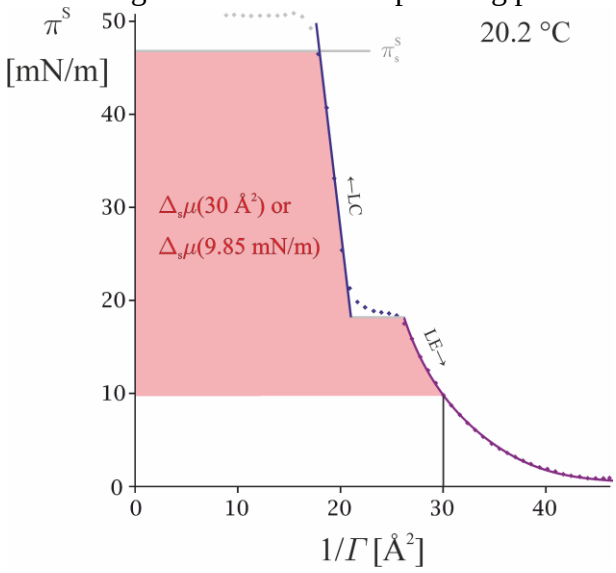

Figure S17. Graphical representation of the chemical potential $\Delta_s\mu$. The surface pressure vs. area isotherm at 20.2 °C is used to compute the value of $\Delta_s\mu$ at π^S = 9.85 mN/m (corresponding to $1/\Gamma$ = 30

Å^2). According to eqn (3), $\Delta_s\mu$ is given by minus the shaded area. π_s^S is the spreading pressure of dodecanol crystals.

For the sake of completeness and for future reference, we also analysed the data for the LE-LC phase transition pressure π_{pt}^S as a function of temperature. Unlike the area per molecule, the surface pressure of the phase transition is unaffected by the desorption and the leakages, so we collected a significant amount of data in the range 10-30 °C, Figure S18. The line in this figure is a quadratic fit. Using the data for π_{pt}^S from Figure S18 and the phase transition areas a_{pt}^{LE} and a_{pt}^{LC} from Table 4, we were able to compute the heat of the phase transition Δh_{pt} through the 2D-Clausius-Clapeyron equation,

$$\frac{d\pi_{pt}^S}{dT} = \frac{\Delta h_{pt}}{T\left(a_{pt}^{LE} - a_{pt}^{LC}\right)}. \qquad (8)$$

The dependence of Δh_{pt} on T that follows from this equation is illustrated in Figure S19.

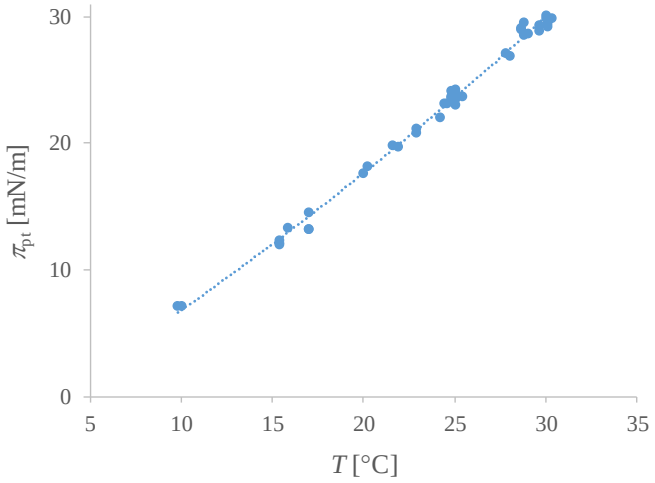

Figure S18. Surface pressure of the LE-LC phase transition as a function of the temperature.

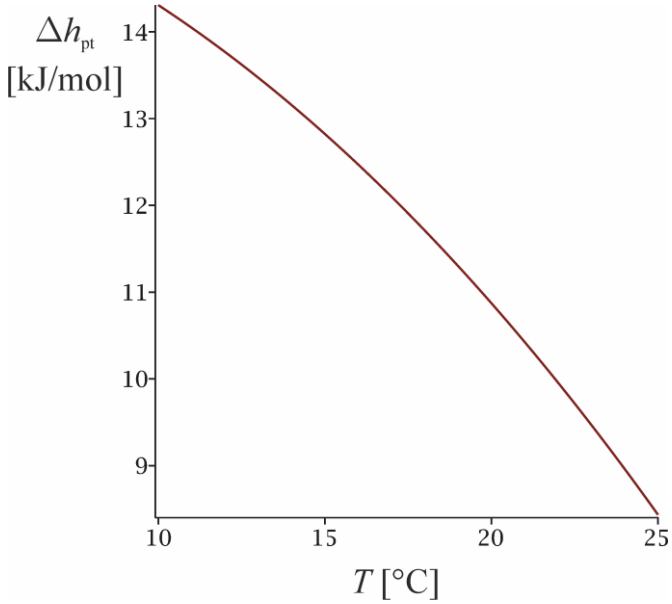

Figure S19. Heat of the LE-LC phase transition.

S5. Leakage through the barrier

The test involved placement of dodecanol crystals in one compartment of the trough and measurement of the surface tension in the other (which should remain clean in the absence of leakage, $\sigma = \sigma_0$), with a barrier separating the two compartments. In the first run (the upper curve in Figure S20), leakage was negligible for 4 minutes, then it caused the observed decrease of σ in the crystal-free compartment. In the second run (lower curve), leakage was immediately apparent. The plateau reached at the 3rd minute corresponds to the LE-LC phase transition.

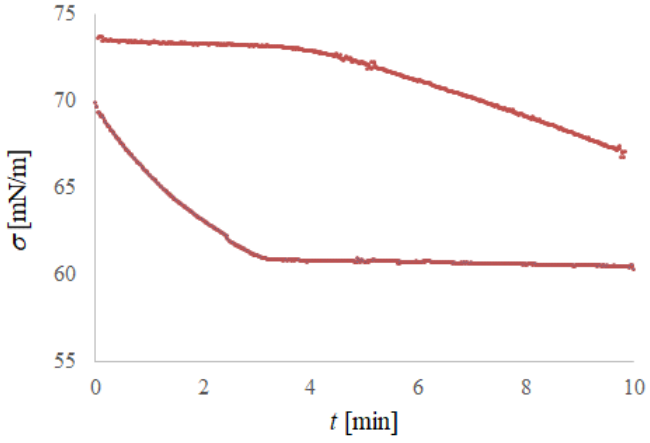

Figure S20. An illustration of random leakage through the movable barrier: in both runs, crystallites are placed in one of the compartments to form an equilibrium spread monolayer at 16 °C. The surface

tension in the second compartment (the surface of which is initially alcohol-free) is measured as a function of time.

S6. Dodecanol – additional data

Here, we present most of our desorption isobars at temperatures from 10 to 23 °C (Figure S21, points). These are compared to the theoretical model (13), with value of τ_d from eqn (24)-(25) and value of τ_{tr} from eqn (11), with the parameters from Table 2.

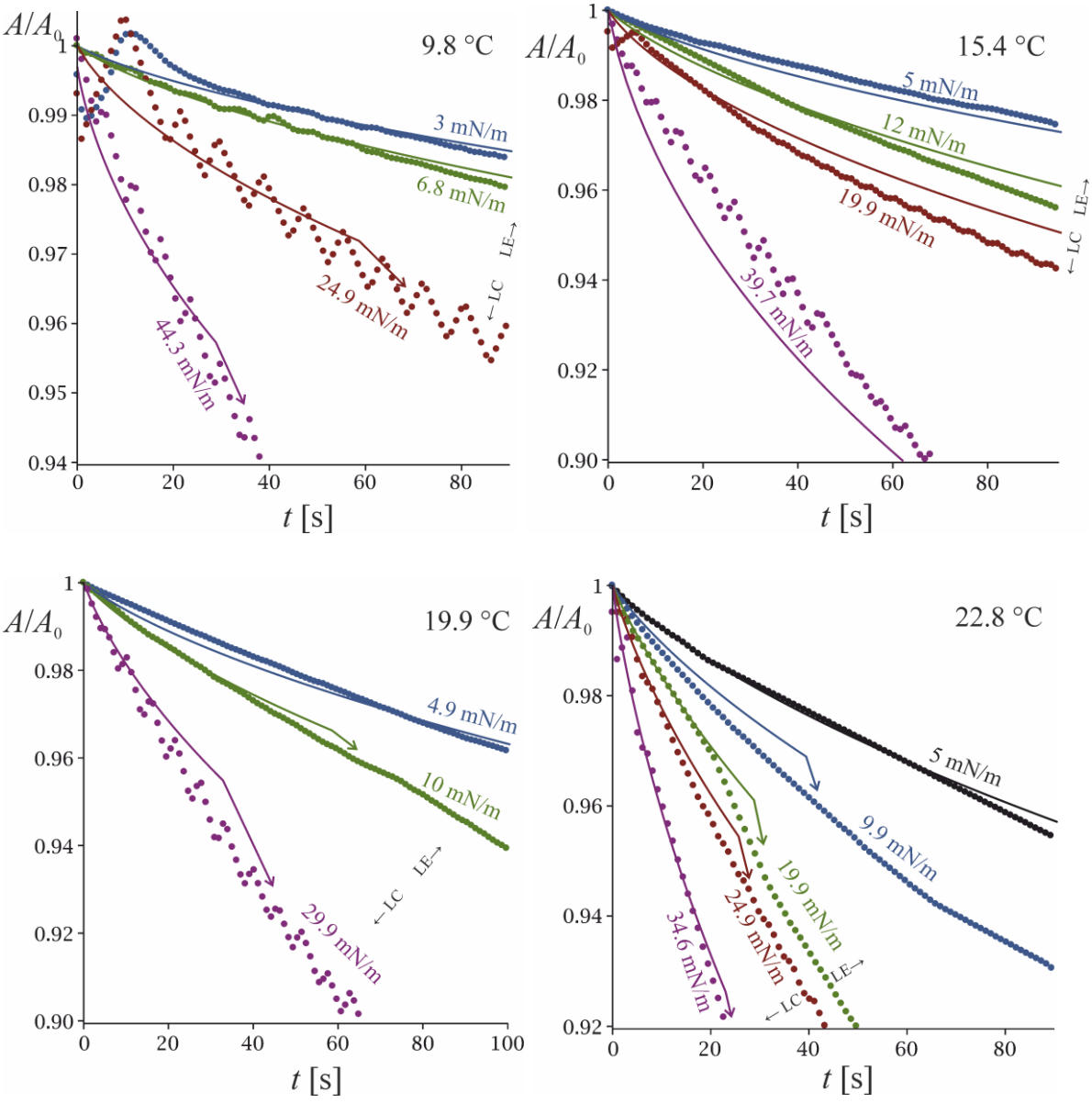

Figure S21. Desorption isobars (relative decrement of the area vs. time) at several fixed surface pressures and temperatures. Solid lines: the theoretical prediction (13) for mixed barrier-diffusion control, with desorption time τ_d linear with $1/\Gamma$ (eqn (24) with K^{LE} and K^{LC} from Table 2).

At higher temperatures (25—30 °C), the desorption is under barrier control as in Figure 9. However, due to the leakages, we were unable to measure the adsorption isotherms at 29 and 30 °C, although we measured desorption isobars. Therefore, in Figure S22, the measured isobars are presented without comparison to theory. We attempted to estimate the required quantities (τ_d and Γ) by extrapolation of the π^S vs. $1/\Gamma$ isotherms in Figure 2 and the τ_d formulae (24)-(25) (which are strictly valid in the range 10-25 °C). Overall, the observed desorption rates seem to be slightly faster than the predicted ones from this extrapolation (as if the real τ_d at 30 °C is by *ca.* 25% smaller than the extrapolated). This might mean that the activation energy E_A^{LE} is underestimated, but might also be due to leakages, evaporation or, in part, to inaccurate extrapolation of the compression isotherm.

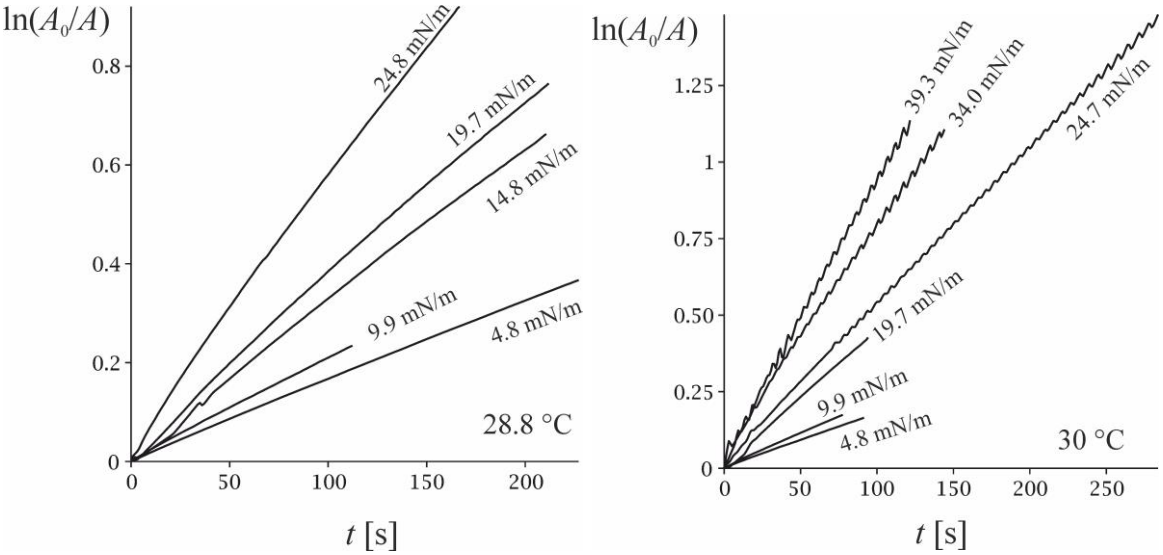

Figure S22. Desorption isobars at 29-30 °C and several fixed surface pressures. The process seems to proceed under barrier control (similarly to the data at 25 °C in Figure 9) for at least 50-100 s, but in the absence of compression isotherm data, we did not try to interpret these data.

In Figure 23, the data of De Keyser and Joos for dodecanol is compared with the theoretical prediction for desorption under pure barrier control (dashed line) and desorption in the τ_d-D regime (solid line). As discussed in sec. 4, in the time range of interest to us (0-200 s), the data indeed suggests barrier control, exactly as our measurements at 25 °C (Figure 9).

t [s]

Figure 23. Desorption isobar by De Keyser and Joos at 8 mN/m (probably 25 °C). Solid line: the theoretical prediction (13) for mixed barrier-diffusion control. Dashed line: pure barrier control, eqn (14). The adsorption Γ and the desorption time τ_d at 8 mN/m were calculated from eqn (16)&(24).

Figure S24 illustrates the dispersion analysis of the fit of the τ_d data in Table 2 with eqn (24)-(25). All values of the parameters K_0 and E_A that fall inside the ellipses "$1.05 \times dev^2_{min}$" will produce dispersion by 5% larger than the minimal.

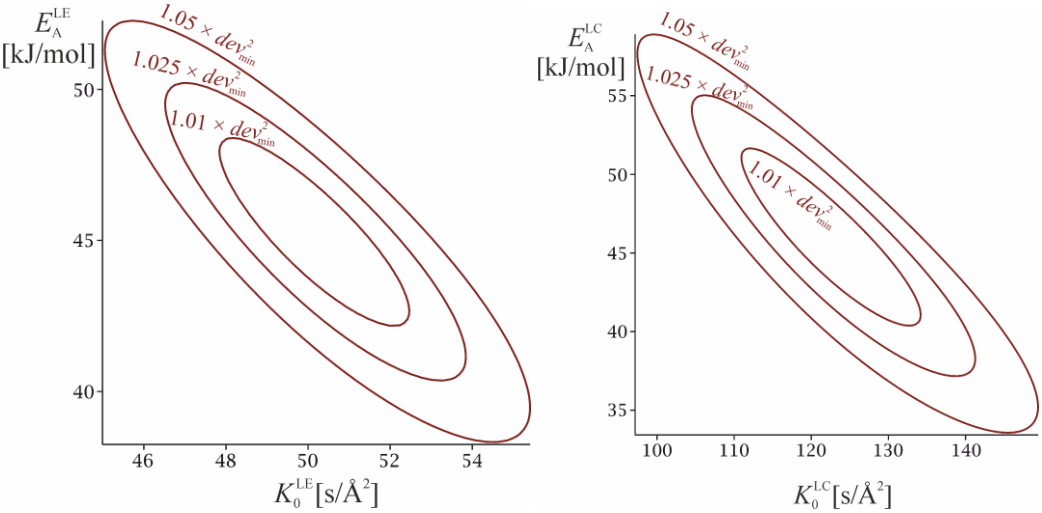

Figure S24. Contour plot of the dispersion of eqn (24)-(25) against the τ_d data in Table 2.

S7. Decanol data

The sticky disc adsorption model predicts a theoretical surface pressure vs. concentration isotherm $\pi^S_{th}(C_{eq}; K_a, \alpha, \beta)$ (a numerical solution to eqn (18)-(19)&(4)). The value of the hard-disc area α is set to the one following from crystallographic data, 16.5 Å^2. The other two parameters are obtained through minimization of the merit function

$$dev^2_\pi(K_a, \beta) = \frac{1}{N-2}\sum_i \left[\pi^S_{th}(C_i; K_a, \beta) - \pi^S_i\right]^2 . \qquad (9)$$

Here, C_i and π^S_i are the experimental surfactant concentrations and surface pressures from ref. [29,38,39,63,82]. We used only low pressure data with π^S < 30 mN/m, since it is likely that at higher surface pressures the monolayer is in the LC state where eqn (18) is invalid, and anyway, the data of Baret et al. are in the range 5—20 mN/m. The result of the regression for the best fit parameters is β = 20.7 and K_a = 39.25 μm, *i.e.* ln(K_a/[m]) = –10.15. These can be compared to β = 14 and ln(K_a/[m]) = –9.8 from ref. [60] (the latter values are not accurate enough for long-chained alcohols such as decanol). The comparison between the data points and the theoretical sticky disc curve with the best fit parameters is shown in Figure S25.

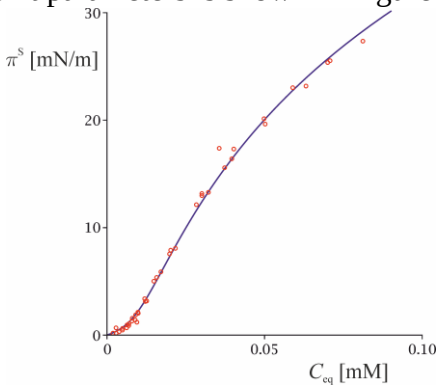

Figure S25. Adsorption isotherm of decanol: data from ref. [29,38,39,63,82] and the best fit with the sticky disc model (18)-(19)&(4), with K_a = 39.25 μm and β = 20.7.

The values obtained for K_a and β allow the computation of Γ and γ^S at each surface pressure of Baret et al. We calculated the adsorptions by solving eqn (18) for Γ; this value of Γ was further substituted in eqn (19) to find the respective surface activity coefficient γ^S. Eqn (4) was then used to calculate C_{eq}. The results for Γ and C_{eq} at the four surface pressures of Baret at al. are given in Table 3 in the main text.

This leaves a single unknown parameter in eqn (13) for the kinetics of desorption: the desorption rate constant τ_d. To find τ_d, eqn (13) has been used to fit the A vs. t data of Baret et al. [6] at each surface pressure. The results are illustrated in Figure S26, and the values of τ_d are summarized in Table 3. An acceleration of the diffusion process is evident at the longest times ($t > t_{max}$) for π^S = 5, 10 and 15 mN/m (discussed also by Baret et al. [6]) – therefore, only the data at $t < t_{max}$ were used for the regression. The times t_{max} where first signs of convective regime are seen were determined iteratively using positive deviations from eqn (13) as a criterion, similarly to the procedure for dodecanol in sec. 3.4. The time of transition is marked with red dots in Figure S26.

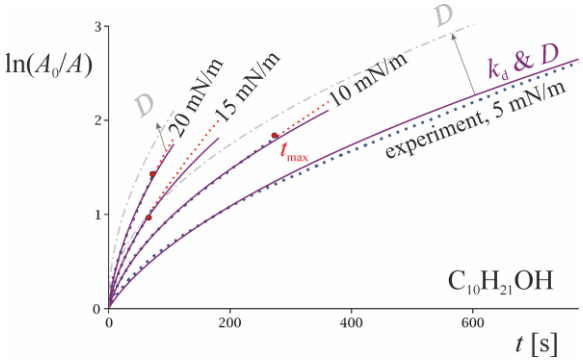

Figure S26. ln(A_0/A) vs t [s] for $C_{10}H_{21}OH$ – data from ref. [6] (dot lines) at 4 surface pressures (5-20 mN/m). Dash-dot lines: *D*-regime, eqn (15), overpredicting the dissolution rate compared to the experiment. Solid lines: fits to the experimental data of eqn (13) for the mixed barrier-diffusion mechanism (τ_d & *D*). The best-fit values of τ_d are listed in Table 3. Acceleration of the desorption process due to convection is evident above certain t_{max} (marked with circles); all data after $t > t_{max}$ were ignored for the fit.